Dating of ultramafic rocks from the Western Alps ophiolites discloses Late Cretaceous subduction ages in the Zermatt-Saas Zone

GISELLA REBAY *†, DAVIDE ZANONI‡, ANTONIO LANGONE§,
PIETRO LUONI‡, MASSIMO TIEPOLO‡ & MARIA IOLE SPALLA‡

*Università degli Studi di Pavia, Dipartimento di Scienze della Terra e dell'Ambiente, Via Ferrata, 1 - 27100 Pavia, Italy
‡Università degli Studi di Milano, Dipartimento di Scienze della Terra 'A. Desio', Via Mangiagalli,
34 - 20133 Milano, Italy
§IGG-CNR U.O.S. - Pavia, Via Ferrata, 1 - 27100 Pavia, Italy

Abstract – The Zermatt-Saas Zone was part of the Middle to Late Jurassic Tethyan lithosphere that underwent oceanic metamorphism during Mesozoic time and subduction during Eocene time (HP to UHP metamorphism). In upper Valtournanche, serpentinite, metarodingite and eclogite record a dominant S2 foliation that developed under 2.5 ± 0.3 GPa and $600 \pm 20\,°C$ during Alpine subduction. Serpentinites contain clinopyroxene and rare zircon porphyroclasts. Clinopyroxene porphyroclasts show fringes within S2 with similar compositions to that of grains defining S2. Zircon cores show zoning typical of magmatic growth and thin fringes parallel to the S2 foliation. These features indicate crystallization of clinopyroxene and zircon fringes during HP syn-D2 metamorphism, related to the Alpine subduction. The U–Pb zircon dates for cores and fringes reveal crystallization at 165 ± 3.2 Ma and 65.5 ± 5.6 Ma, respectively. The Middle Jurassic dates are in agreement with the known ages for the oceanic accretion of the Tethyan lithosphere. The Late Cretaceaous - Paleocene dates suggest that the Zermatt-Saas Zone experienced high-pressure to ultra-high-pressure (HP–UHP) metamorphism at *c.* 16 Ma earlier than previously reported. This result is in agreement with the evidence that in the Western Alps the continental Sesia-Lanzo Zone reached the subduction climax at least from 70 Ma and was exhumed during ongoing oceanic subduction. Our results are further evidence that the Zermatt-Saas ophiolites diachronically recorded heterogeneous HP–UHP metamorphism.

Keywords: serpentinites, subduction metamorphism, microstructural analysis, U–Pb dating, Tethys opening

1. Introduction

Ophiolites represent oceanic remnants in mountain chains and their tracking, together with the reconstruction of their structural and metamorphic history, is still one of the basic tools for understanding the dynamics of collisional chain development. In the Alps, the key significance of ophiolites in geodynamics was long understood before the birth of plate tectonics (e.g. Brongniart, 1813; Argand, 1911; Steinmann, 1927). Since the first geological research within the Alps ophiolites from the Piedmont zone have been a favourable investigation object (Dal Piaz, 2010), especially in the exploration of deformation and mineral transformation histories of high-pressure (HP) and ultra-high-pressure (UHP) units of the Zermatt-Saas Zone (ZSZ). In the last years a debate developed on this portion of the Piedmont zone, regarding whether the pressure–temperature (*P–T*) conditions registered by ZSZ rocks are largely uniform or if different portions of ZSZ recorded different *P–T*-peak conditions and underwent different exhumation paths over different time spans (e.g. Lapen *et al.* 2003; Li, Rahn & Bucher, 2004; Angiboust *et al.* 2009; Groppo, Beltrando & Compagnoni, 2009; Angiboust & Agard, 2010; de Meyer *et al.* 2014; Skora *et al.* 2015; Weber & Bucher, 2015; Weber *et al.* 2015). This last view has been recently reinforced by multiscalar structural and petrological analysis supported by detailed field mapping (Rebay, Spalla & Zanoni, 2012; Weber & Bucher, 2015; Zanoni, Rebay & Spalla, 2016). The multiscalar analytical approach could be deeply reinforced by careful geochronological work, and becomes important in understanding the critical size of oceanic units able to record a homogeneous structural and metamorphic evolution during burial and exhumation paths in a subduction system. This means identifying volumes that have completed, remaining intact, their tectonic trajectory during a given time span. In addition, this allows light to be shed on how the coupling and decoupling of tectonic units can occur in the subduction mantle wedge or in the orogenic wedge during continental collision (e.g. Cloos, 1982; Chemenda *et al.* 1995; Stoeckhert & Gerya, 2005; Baumann, Gerya & Connolly, 2010; Roda, Marotta & Spalla, 2010; Gerya, 2011; Malatesta *et al.* 2012, 2016; Roda,

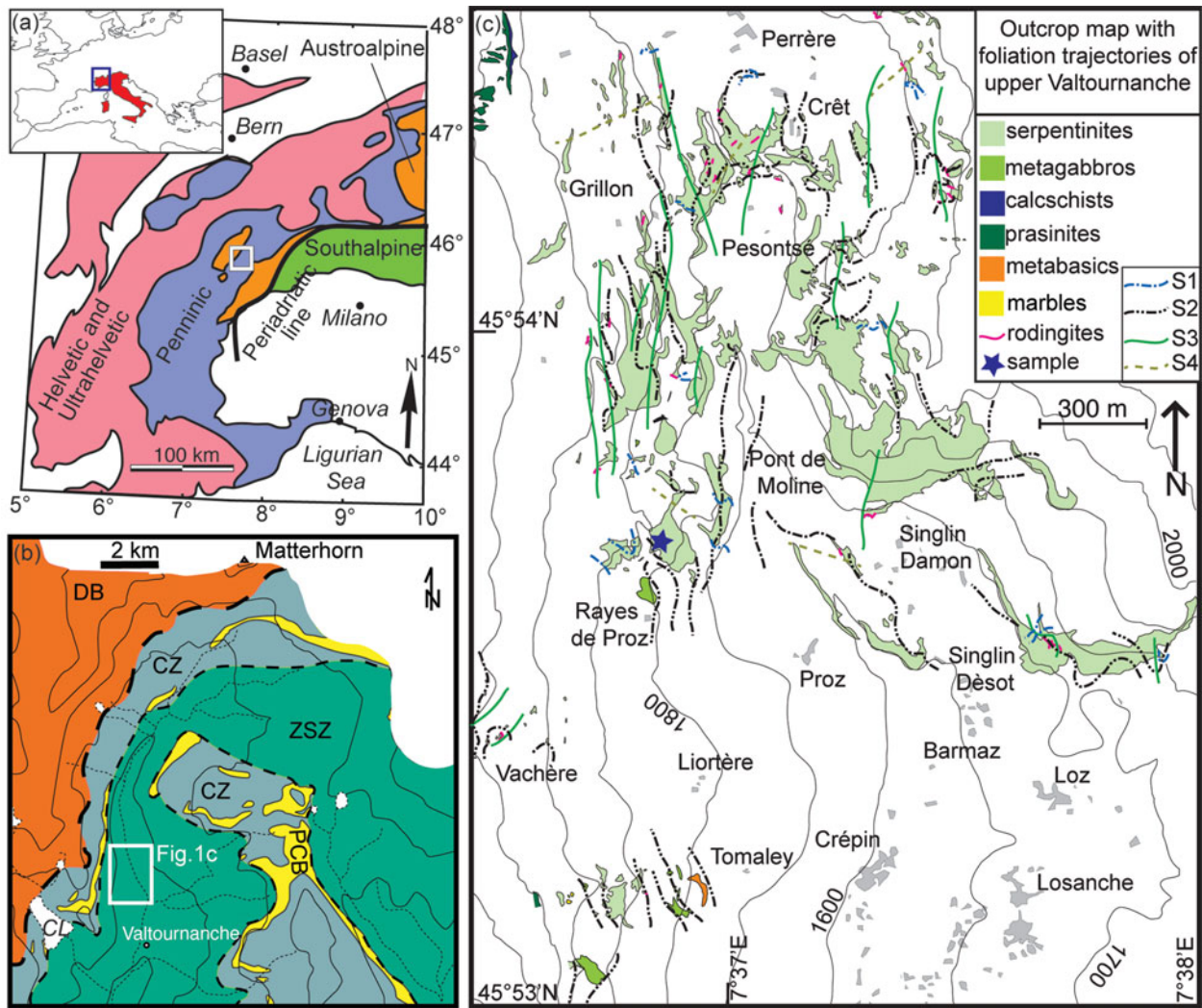†Author for correspondence: gisella.rebay@unipv.it

Figure 1. (Colour online) Geological and structural outline of the upper Valtournanche. (a) Tectonic sketch map of the Western Alps and its location within Europe and the Mediterranean region. (b) Interpretative tectonic sketch of the upper Valtournanche redrawn from the geotectonic map of the Aosta Valley (De Giusti *et al.* 2003); area indicated by the thick white square in (a). ZSZ – Zermatt-Saas Zone; PCB – Pancherot-Cime Bianche-Bettaforca unit; CZ – Combin Zone; DB – Dent Blanche nappe; CL – Cignana Lake. (c) Outcrop map with the foliation trajectories of the metaophiolites of the upper Valtournanche (ZSZ), synthesized from an original mapping (unpublished) at 1:5000 scale. Relative chronology of superimposed foliation is shown in the legend. Topography redrawn from the technical map of the Val d'Aosta Regional Administration without hydrography.

Spalla & Marotta*, 2012). Different subduction dynamics can result in the formation of tectonic units with different sizes and different ages, sharing a coherent structural and metamorphic evolution.

The main goal of this contribution is to present new age data on microstructural sites selected on the basis of a well-defined chronology of superimposed structures and metamorphic imprints at the regional scale, and to implement the chronological outline of eclogitized ZSZ ophiolites from the upper Valtournanche serpentinites in order to take some steps towards a better constrained regional framework.

2. Geological setting

The ZSZ, together with the Combin Zone (CZ), represents a Tethyan ocean relict that comprises rocks

variously affected by oceanic- and subduction-related metamorphism, which now are transposed along the axial belt of the Western Alps (Caron *et al.* 1984; Reddy, Wheeler & Cliff, 1999; Dal Piaz, 2010; Spalla *et al.* 2010). These two zones are tectonically sandwiched between the continental Monte Rosa (beneath) and Dent Blanche – Sesia Lanzo nappes (above) that belong to the Penninic and Austroalpine domains, respectively (e.g. Bearth, 1967; Polino, Dal Piaz & Gosso, 1990). The ZSZ (Fig. 1a, b) underlies the CZ and, due to their different lithostratigraphic and metamorphic features, these two units have been interpreted as deriving from the oceanic lithosphere and from the ocean–continent transition zone, respectively (e.g. Dal Piaz & Ernst, 1978; Dal Piaz *et al.* 1981). In the upper Valtournanche, ZSZ and CZ are separated by slices of pre-Alpine continental rocks and schists deriving

Table 1. Summary of age data for Western Alps ophiolites and peak *P–T* conditions for Zermatt-Saas Zone

Key	Locality	Rock	Dating method; mineral	Age (Ma)	Peak *P–T* conditions	Event	Reference
	Zermatt-Saas Zone						
	Alallin glacier	Metagabbro	U–Th–Pb; zircon	164.0 ± 2.7		Emplacement	Rubatto, Gebauer & Fanning, 1998
	Mellichen	Leucogabbro	U–Th–Pb; zircon	163.5 + 1.8		Emplacement	Rubatto, Gebauer & Fanning, 1998
	Tasch Valley	Metasediment	U–Th–Pb; zircon	153–173		Deposition	Rubatto, Gebauer & Fanning, 1998
	Cignana	Metasediment	U–Th–Pb; zircon	161 ± 11		Deposition	Rubatto, Gebauer & Fanning, 1998
3	Triftji	Metapelite	Rb–Sr; garnet phengite inclusion	44.86 ± 0.49 to 43.6 ± 1.8		Prograde	de Meyer *et al.* 2014
3	Triftji	Metapelite	Rb–Sr; phengite (matrix)	40.01 ± 0.51 to 39.5 ± 1.1		Prograde	de Meyer *et al.* 2014
5	Pfulwe	Eclogite	Lu–Hf; garnet	48.9 ± 2.8		Prograde	Skora *et al.* 2015
12	Chamois	Eclogite	Lu–Hf; garnet	52.6 ± 1.7		Prograde	Skora *et al.* 2015
8	Trockener Steg	Eclogite (continental)	Lu–Hf; garnet-whole-rock	56.5 ± 2.7 to 58.2 ± 1.4		Prograde	Weber *et al.* 2015
11	Cignana	Eclogite	Lu–Hf; garnet-omphacite-whole-rock	48.8 ± 2.1		Prograde	Lapen *et al.* 2003
11	Cignana	Eclogite	REE; garnet	70–80		Prograde	Skora *et al.* 2009
9	Breuil	Metabasalts and metagabbros			0.8–1.2 GPa, 420–520 °C	HP	Ernst & Dal Piaz, 1978
2	Allalinhorn	Metagabbro			1.5 GPa, 570–700 °C	HP	Chinner & Dixon, 1973
2	Allalinhorn	Metagabbro			2.5 GPa, 610 °C	HP	Bucher & Grapes, 2009
2	Allalinhorn	Metabasalts			2.3–2.5 GPa, 530–555 °C	HP	Angiboust *et al.* 2009
6	Zermatt	Metabasites			1.4 GPa, 600 °C	HP	Oberhänsli 1980
6	Zermatt	Metabasites			1.75–2.0 GPa, 550–600 °C	HP	Barnicoat 1988
8	Trockener Steg	Eclogite (continental)			2.2–2.3 GPa, 515–645 °C	HP	Weber & Bucher, 2015
8	Trockener Steg	Eclogite			2.2–2.3 GPa, 450–550 °C	HP	Weber & Bucher, 2015
7	Lichenbretter	Serpentinites			2.0–2.5 GPa, 600–650 °C	HP	Li, Rahn & Bucher, 2004
7	Riffelhorn-Gornergrat	Serpentinites			2.0–2.5 GPa, 600–650 °C	HP	Li, Rahn & Bucher, 2004
13	St Jacques	Eclogite	Lu–Hf; garnet	39.2 ± 1.6	0.8–1.2 GPa, 420–520 °C	HP	Skora *et al.* 2015; Ernst & Dal Piaz, 1978
5	Pfulwe	Eclogite	Lu–Hf; garnet-whole- rock	48.9 ± 4.8	1.75–2.0 GPa, 550–600 °C	HP	Mahlen *et al.* 2006; Barnicoat & Fry 1986
1	Saas Fee	Eclogite	Lu–Hf; garnet	38.1 ± 2.7 to 40.7 ± 1.8		HP	Skora *et al.* 2015
1	Saas Fee	Metagabbro			2.5 GPa, 650 °C	HP	Meyer 1983
1	Saas Fee	Metabasites			2.5 GPa, 650 °C	HP	Bucher & Frey 1994
10	Valtournenche	Serpentinites			2.2–2.8 GPa, 600 °C	HP–UHP	Rebay, Spalla & Zanoni, 2012
10	Valtournenche	Rodingites			2.3–2.8 GPa, 580–660 °C	HP–UHP	Zanoni, Rebay & Spalla, 2016
5	Pfulwe	Metabasalts			2.5–3.0 GPa, 550–600 °C	UHP	Bucher *et al.* 2005
3	Mellichen	Leucogabbro	U–Th–Pb; zircon	48.8 ± 2.9		UHP	Rubatto, Gebauer & Fanning, 1998
3	Mellichen	Leucogabbro	U–Th–Pb; zircon	40.3 ± 9.2		UHP	Rubatto, Gebauer & Fanning, 1998
3	Mellichen	Metabasalts			2.5–3.0 GPa, 550–600 °C	UHP	Bucher *et al.* 2005
11	Cignana	Eclogite	Sm–Nd; garnet	40.6 ± 2.6	2.6–3.0 GPa, *c.* 600 °C	UHP	Amato *et al.* 1999; van der Klauw, Reinecke & Stöckhert, 1997

Table 1. Continued

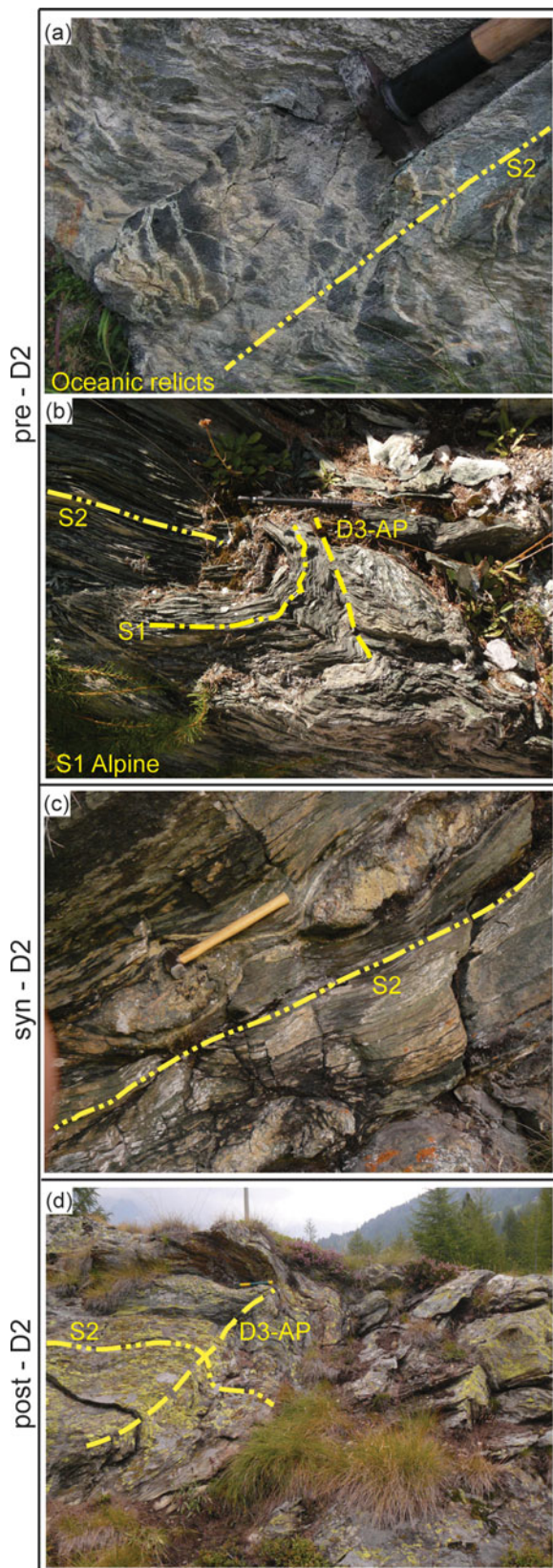| Key	Locality	Rock	Dating method; mineral	Age (Ma)	Peak P–T conditions	Event	Reference
11	Cignana	Eclogite	Sm–Nd; garnet	52 ± 18		UHP	Bowtell, Cliff & Barnicoat, 1994
11	Cignana	Eclogite	U–Th–Pb; zircon	44.1 ± 0.7		UHP	Rubatto, Gebauer & Fanning, 1998
11	Cignana	Metasediment	U–Th–Pb; zircon	44.1 ± 0.7	2.7–3.0 GPa, 600 °C	UHP	Rubatto, Gebauer & Fanning, 1998; Reinecke 1995, 1998
11	Cignana	Metasediments	Ar–Ar; garnet phengite inclusion	43.2 ± 1.1 44.4 ± 1.5		UHP	Gouzu *et al.* 2006; Reinecke, 1991
11	Cignana	Quarzite	Rb–Sr; phengite	40.7 ± 0.1	2.6–2.8 GPa, 590–630 °C	UHP–retrograde	Skora *et al.* 2015; Reinecke, 1991
1	Saas Fee	Calcschists	Rb–Sr; phengite	39.5 ± 0.1		HP–retrograde	Skora *et al.* 2015
	Cignana	Quarzite	Rb–Sr; whole-rock-phengite	38 ± 2		Retrograde	Amato *et al.* 1999
	Tasch Valley	Metapelite	Rb–Sr; whole-rock-phengite	38 ± 2		Retrograde	Amato *et al.* 1999
	Cignana	Metasediments	Ar–Ar; phengite (matrix)	42–37 (plateaux age)		Retrograde	Gouzu *et al.* 2006
	Cignana (UU)	Metabasite	K–Ar; phengite	38–41		Retrograde	Gouzu *et al.* 2016
	Cignana (UU)	Metasediments	K–Ar; phengite	38–41		Retrograde	Gouzu *et al.* 2016
	Cignana (LU)	Eclogite	K–Ar; paragonite	37–38		Retrograde	Gouzu *et al.* 2016
	Cignana (LU)	Eclogite	K–Ar; phengite	37–38		Retrograde	Gouzu *et al.* 2016
Combin Zone							
	Cignana (LCU)	Pelitic shist	K–Ar; phengite	39–41		Retrograde	Gouzu *et al.* 2016
	Cignana (LCU)	Piemontite shist	K–Ar; phengite	39–41		Retrograde	Gouzu *et al.* 2016
	Cignana (LCU)	Eclogite	K–Ar; paragonite	39–41		Retrograde	Gouzu *et al.* 2016
	Cignana (LCU)	Mn-rich metasediment	K–Ar; phengite	39–41		Retrograde	Gouzu *et al.* 2016
	Cignana	Calcschists	K–Ar; phengite	36–40		Retrograde	Gouzu *et al.* 2016
Antrona							
	Guggilihorn	Metabasics	Pb–U; zircon	155 ± 1.6		Emplacement	Liati, Froitzheim & Fanning, 2005
	Passo del Mottone	Metabasics	Pb–U; zircon	158 ± 17		Emplacement	Liati, Froitzheim & Fanning, 2005
	Quarata	Metabasics	Pb–U; zircon	155.6 ± 2.1		Emplacement	Liati, Froitzheim & Fanning, 2005
	Hinterrhein area	Metagabbro	Pb–U; zircon	161 ± 3.9		Emplacement	Liati, Froitzheim & Fanning, 2005
	Passo del Mottone	Amphibolite	Pb–U; zircon	38.5 ± 0.7		HP	Liati, Froitzheim & Fanning, 2005
	Alpe la Balma	Eclogite	Lu–Hf; garnet-whole-rock	42–45.5		HP	Herwartz *et al.* 2008
Monviso							
	Vernè (Val Varaita)	Meta-plagiogranite	U–Pb; zircon	152 ± 2		Emplacement	Lombardo, Rubatto & Castelli, 2002
	Lago Superiore	Eclogite	U–Pb; zircon	163 ± 2		Emplacement	Rubatto & Hermann, 2003
	Lago Superiore	Eclogite	Lu–Hf; garnet-whole-rock	49.2 ± 1.2		Prograde–HP	Duchêne *et al.* 1997
	Lago Superiore	Metamorphic vein	U–Pb; zircon	45 ± 1		HP	Rubatto & Hermann, 2003
	Lago Superiore	Eclogitic mylonite	Rb–Sr; phengite	41.6 ± 0.4		HP	Cliff, Barnicoat & Inger, 1998
	Lago Superiore	Eclogitic mylonite	Sm–Nd; garnet and clinopyroxene	60 ± 12		HP	Cliff, Barnicoat & Inger, 1998
	Lago Superiore	Eclogitic metagabbros	Ar–Ar; phengite	48–53 Ma		HP	Monié & Philippot, 1989
Voltri Group							
		Eclogite	Ar–Ar; phengite	49.0 ± 0.4		HP	Federico *et al.* 2005
		Blueschists	Ar–Ar; phengite	43.5 ± 1.7		HP–retrograde	Federico *et al.* 2005
		Metasediments	Ar–Ar; muscovite	32.9 ± 0.8		Retrograde	Federico *et al.* 2005

Figure 2. (Colour online) (a) Net of whitish amphibole-clinopyroxene-bearing veins intersected by S2 foliation. Hammer for scale. (b) S1 foliation folded during the development of D2 and post-D2 deformation stages. D2 is accompanied by the development of the S2 foliation and D3 produced only a folding (D3-AP = D3 axial plane). Pencil for scale. (c) Pervasive S2 foliation that wraps around rodingite boudins. Hammer for scale. (d) Metre-sized D3 fold. Hammer for scale.

from Permian–Cretaceous sediments (Dal Piaz, 1999, 2010). The main difference between ZSZ and CZ is the dominant metamorphic imprint: eclogite facies in the first and greenschist facies in the second. Despite the pervasive greenschist re-equilibration, CZ rocks preserve blueschist facies relics, whereas remnants of eclogite facies assemblages have never been detected, even in the less-deformed rocks (Cartwright & Barnicoat, 2002; Dal Piaz, 1974; Dal Piaz & Ernst, 1978; Ring, 1995). The greenschist facies assemblages are extremely localized in the mostly eclogitized rocks of ZSZ and are mainly interpreted as exhumation-related metamorphic imprints (e.g. Cartwright & Barnicoat, 2002; Ernst & Dal Piaz, 1978); scattered relics pre-dating the eclogite facies peak preserve blueschist facies mineral assemblages (e.g. Chinner & Dixon, 1973; Ernst & Dal Piaz, 1978). Metabasic rocks are the most explored to determine the Alpine metamorphic evolution of this portion of the Tethys ocean and results give a wide span of P–T values in different portions of ZSZ: 2.5–3.0 GPa and 550–600 °C (Bucher et al. 2005); 1.9–2.2 GPa and 530–600 °C (Dale et al. 2009); and, south of the Aosta-Ranzola fault (St Marcel valley), 2.1 ± 0.3 GPa and 550 ± 60 °C (Martin et al. 2008). The metagabbros of the Swiss portion of the ZSZ record peak conditions of 2.5–2.8 GPa and 600–610 °C (Bucher & Grapes, 2009) or alternatively 1.9–2.2 GPa and 500–580 °C (Dale et al. 2009). Pressures from 2.7 to >3.2 GPa and temperatures of 590–630 °C are estimated at Lago di Cignana (e.g. Reinecke, 1991, 1998; van der Klaauw, Reinecke & Stöckhert, 1997; Groppo, Beltrando & Compagnoni, 2009), where microdiamonds have also been found in oceanic metasedimentary rocks (Frezzotti et al. 2011). Peak P–T estimates from serpentinites of the Swiss side are at 2.0–2.5 GPa and 600–650 °C (Li, Rahn & Bucher, 2004), whereas in the Italian side they are at 2.2–2.8 GPa and 580–620 °C (Rebay, Spalla & Zanoni, 2012). The latter estimates have recently been supported by P–T peak conditions determined by thermodynamic modelling of the hosted eclogitized rodingites (2.3–2.8 GPa and 580–660 °C; Zanoni, Rebay & Spalla, 2016). All these P–T estimates led to the inference of trajectories indicating the occurrence of heterogeneous metamorphic evolutions in different portions of ZSZ. In contrast, different authors have suggested a homogeneous evolution for the entire ZSZ based on the assemblages from metabasites and calcschists, with peak conditions at 2.3 ± 0.1 GPa and 540 ± 40 °C (Angiboust et al. 2009; Angiboust & Agard, 2010). In addition, part of the Monviso ophiolite has been interpreted as forming a single unit with the ZSZ, which would consist of a continuous slab, recording a coherent metamorphic evolution during the Alpine subduction (Angiboust et al. 2012). This interpretation differs from that of previous authors, suggesting that the Monviso is a complex of eclogitized ophiolitic slices accreted during the final stages of their exhumation on the basis of contrasted P–T trajectories (Schwartz et al. 2000; Guillot et al. 2004). Consistent with a
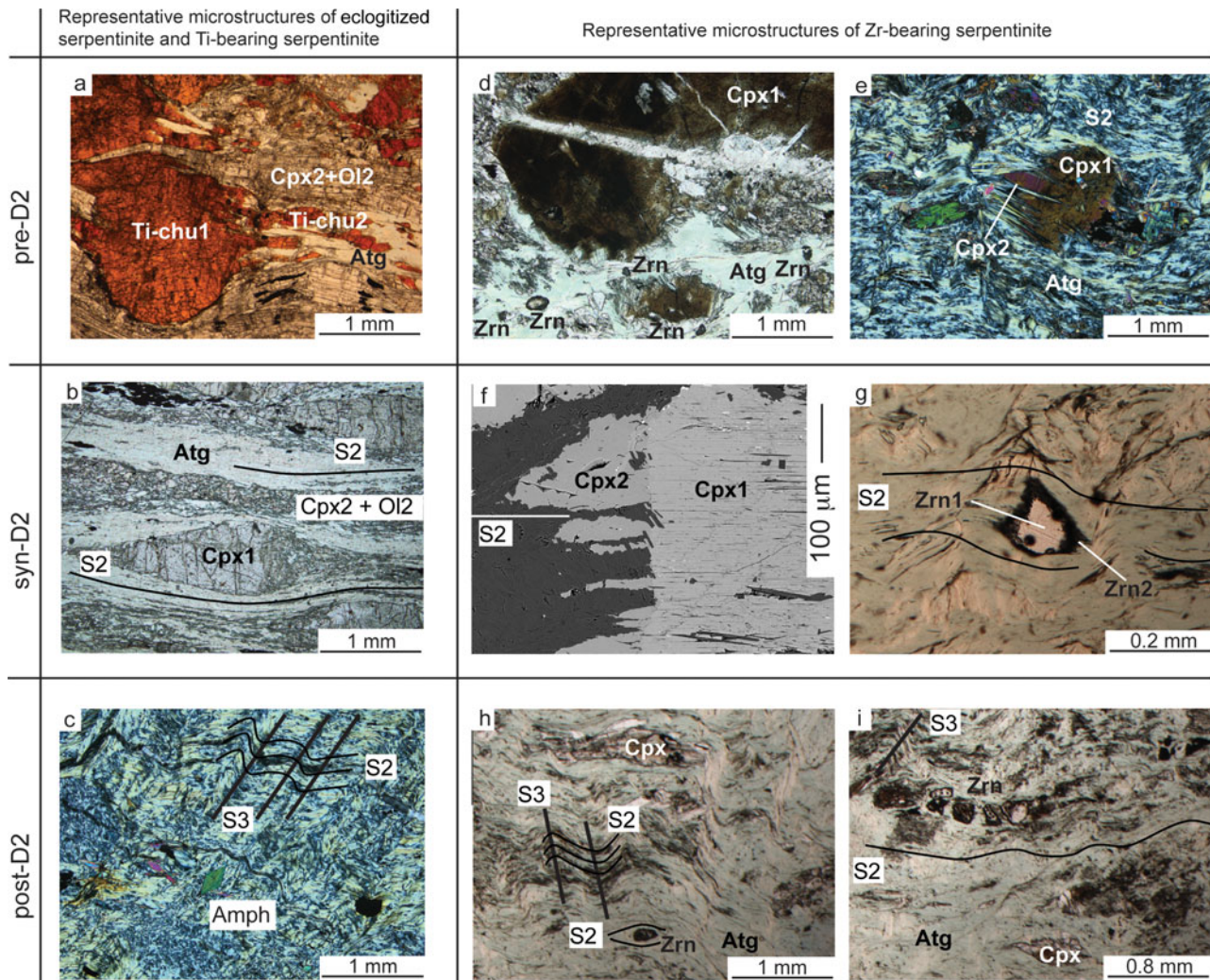
Figure 3. (Colour online) Microphotographs of (a–c) eclogitized and Ti-clinohumite-bearing serpentinite, and (d–i) of the zircon bearing eclogitized serpentinite sample. (a) Ti-clinohumite1 porphyroclasts (Ti-chu1) wrapped by S2 defined by Ti-clinohumite2 (Ti-chu2), olivine2 (Ol2), clinopyroxene2 (Cpx2) and antigorite (Atg); (b) syn-D2 mylonite with a clinopyroxene1 porphyroclast (Cpx1) and banded S2 foliation defined by clinopyroxene2 (Cpx2), olivine2 (Ol2) and antigorite (Atg); (c) S2 defined by antigorite overprinted by an incipient S3 crenulation cleavage; amphibole (Amph) porphyroblasts (note basal sections) show SPO parallel to S3; (d) large field view of the zircon-bearing serpentinite with a large, fractured, clinopyroxene (Cpx1) porphyroclast (dark) wrapped by S2, which is defined by antigorite (Atg), olivine2 and clinopyroxene2 (in the lower part there are five zircon porphyroclasts, Zrn); (e) clinopyroxene1 porphyroclast (Cpx1) with clinopyroxene2 (Cpx2) spikes parallel to S2, here defined by antigorite (Atg); (f) SEM backscattered image of a large clinopyroxene1 (Cpx1) with spikes of clinopyroxene2 (Cpx2) parallel to S2; (g) zircon (Zrn1) wrapped by antigorite defining S2, showing zircon2 (Zrn2) growths parallel to S2 (see zircon shape in CL image in Fig. 4c, h) clinopyroxene (Cpx) and zircon (Zrn) porphyroclasts wrapped by S2 overprinted by S3 crenulation cleavage; and (i) large zircon boudinaged within S2 that wraps a small clinopyroxene1 (Cpx1) porphyroclast, overprinted by S3 crenulation cleavage.

heterogeneous metamorphic evolution, Alpine ages indicate a wide time interval of re-equilibration during subduction of the ZSZ rocks and associated continental slivers (Table 1) of 80–38 Ma, with ages interpreted as referred to peak conditions as 52–38 Ma (Bowtell, Cliff & Barnicoat, 1994; Rubatto, Gebauer & Fanning, 1998; Dal Piaz *et al.* 2001; Skora *et al.* 2009, 2015; Springer *et al.* 2009; de Meyer *et al.* 2014; Weber *et al.* 2015). Moreover, considering only U–Pb zircon methods, such ages cluster at *c.* 48–40 Ma (Table 1). Protolith ages indicate gabbro emplacement at 167–161 Ma and sediment deposition during 170–150 Ma (Table 1; Rubatto, Gebauer & Fanning, 1998).

3. Mesostructure

Along the upper Valtournanche valley, between Valtournanche village and Perrère hydroelectric plant, serpentinite is the dominant lithotype. Hectometre-sized metagabbro bodies and up to a few metres thick rodingite boudins and dykes are associated with serpentinites, together with marbles and calc-schists (Fig. 1c). The dominant fabric in serpentinites, metagabbros and rodingites is the tectonitic to mylonitic S2 foliation, and less-deformed domains contain textural and structural pre-D2 relics (Fig. 2a–c). S2 is in turn overprinted by two groups of superimposed ductile structures (D3 and D4); all ductile

Table 2. Trace element composition (ppm) of clinopyroxene and zircon (zircon grain names refer to Fig. 5)

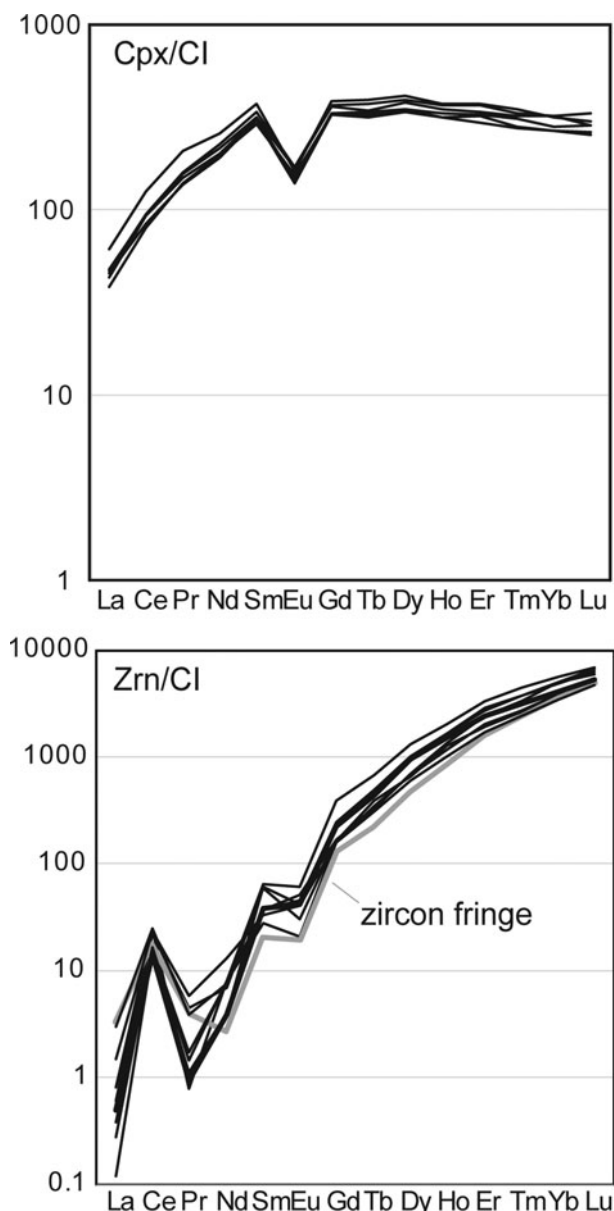| Mineral Grain Position	Cpx						Zrn								
	1 Core	1 Core	1 Rim	2 Core	2 Core	3 Core	18_1a Core dark	18_1b Core light	18_03 Fringe	18_03 Core	18_05 Core	18_06a Core dark	18_06b Core light	18_11a Core light	18_11b Core dark
Li	18.4	15.7	15.4	13.6	14.5	16.6	<1.84	2.32	<1.26	<0.00	3.35	<0.00	<2.07	<1.66	<0.00
Be	1.15	1.48	4.65	2.43	<2.26	2.83	27.1	<0.00	<14.04	<11.40	<12.41	<0.00	<0.00	<12.42	<8.76
B	4.94	3.72	8.98	6.97	3.97	4.27	<8.03	<9.23	16.48	14.18	66.13	14.84	11.73	23.48	35.83
Na	6039	6187	5547	6370	5359	7102	10.8	136.0	22.3	103.6	9.9	15.6	30.3	<2.51	120.8
Sc	138	139	130	166	155	154	492	485	390	448	490	423	432	444	406
Ti	2390	2602	1846	2707	2450	2296	37.9	60.2	14.7	<8.35	<10.67	12.6	46.6	20.1	36.1
V	102	103	107	74.2	74.7	70.7	2.72	<1.50	6.15	5.26	<1.88	<1.39	1.59	<1.29	<1.37
Cr	1470	1830	538	84.0	79.4	85.0	24.7	<15.74	108.0	<13.78	<18.42	<12.24	13.8	<12.46	<13.83
Co	35.7	34.9	31.3	41.3	36.1	37.4	0.67	<0.40	7.69	0.4	2.04	<0.21	1.96	<0.27	0.7
Ni	343	356	325	234	236	254	<1.69	<1.59	131	2.94	7.44	4.06	29.7	<1.16	2.63
Zn	114	119	109	190	144	135	<6.64	32.6	<6.61	5.28	<6.59	<4.99	<3.18	<5.07	<4.57
Rb	0.077	<0.030	0.109	0.126	<0.035	0.059	0.36	0.47	<0.25	0.44	<0.23	0.23	0.7	0.91	0.76
Sr	12.4	12.4	12.5	13.1	15.0	13.4	0.75	1.07	0.42	0.73	0.84	0.44	0.55	0.58	0.88
Y	402	410	483	465	407	449	1919	1828	1474	2381	2155	2693	1687	2651	3245
Zr	118	117	93	137	118	124	—	—	—	—	—	—	—	—	—
Nb	0.273	0.624	0.333	0.392	0.404	0.762	49.8	46.4	36.7	37.5	37.0	31.0	33.7	33.9	28.2
Ba	0.039	<0.00	0.61	<0.064	0.108	0.409	<0.00	<0.243	0.36	<0.00	<0.00	0.2	0.22	0.2	<0.37
La	10.6	11.2	14.5	11.0	9.1	10.2	0.191	0.14	0.78	0.116	0.7	0.065	0.347	0.028	0.088
Ce	50.9	55.8	76.4	57.3	48.2	56.0	14.7	13.4	10.6	8.6	14.9	9.8	14.2	9.2	10.1
Pr	12.2	13.2	18.4	14.2	12.3	14.0	0.07	0.396	0.354	0.083	0.34	0.155	0.516	0.1	0.127
Nd	86.6	90.4	116	102	89.3	97.1	3.63	3.13	1.21	1.76	3.37	3.55	5.97	1.79	3.64
Sm	44.7	45.9	54.6	49.5	43.1	46.6	4.04	8.59	3.03	5.55	5.46	5.52	4.93	9	9.58
Eu	7.74	8.19	9.05	9.5	8.56	9.33	1.16	1.69	1.09	2.33	2.88	2.56	2.27	2.33	3.41
Gd	64.5	65.5	75.4	71.7	64.4	70.5	30.9	32.1	25.5	44.2	33.0	48.2	31.5	48.8	75.5
Tb	11.5	12.3	14.4	13.7	11.8	12.5	12.64	14.2	8.07	15.8	12.05	17.2	11.3	18.1	24.3
Dy	82.5	85.0	100.1	95.5	84.4	92.7	163	161	115	231	167	245	147	243	319
Ho	17.6	17.5	20.9	20.5	18.3	19.4	66.1	70.7	48.0	84.7	74.9	91.4	56.6	92.7	113
Er	47.0	50.8	58.9	58.2	51.5	53.5	321	309	256	386	386	459	273	432	527
Tm	6.66	6.77	8.41	8.01	7.5	7.79	66.0	64.5	57.4	76.6	79.9	91.8	59.1	90.1	108
Yb	43.1	43.5	51.2	51.8	46.0	52.0	621	575	588	670	806	808	562	796	921
Lu	6.16	6.35	7.28	8.04	6.94	6.99	127	114	121	130	145	161	114	154	166
Hf	5.46	5.36	5.39	6.24	5.15	6.78	12546	12504	11558	11337	12349	10941	10415	11184	11229
Ta	0.0145	0.0299	0.0233	0.0075	0.054	0.034	0.510	0.319	2.03	0.162	0.63	0.456	1.1	0.455	0.767
Pb	0.286	0.219	0.331	0.283	0.286	0.329	0.210	0.470	0.430	0.400	0.780	0.231	0.232	0.263	0.310
Th	0.0462	0.053	0.0365	0.082	0.102	0.0324	6.45	4.15	4.16	4.46	12.57	7.77	15.43	7.29	9.22
U	0.0044	<0.0063	0.0116	0.017	0.0077	0.0468	10.4	8.9	12.7	9.1	16.5	14.0	17.6	14.5	15.8
Th/U							0.62	0.46	0.33	0.49	0.76	0.55	0.88	0.50	0.58

Figure 4. REE patterns (chondrite normalized) of clinopyroxene and zircon cores.

structures were mapped with spatial continuity (Fig. 1c) by means of multiscale structural analysis (Rebay, Spalla & Zanoni, 2012; Zanoni *et al.* 2012; Zanoni, Rebay & Spalla, 2016). S2 locally is mylonitic and associated with a tight to isoclinal folding that is characterized by a shallow west-dipping axial plane and a NNW–SSE shallow plunging axis. Contacts between serpentinites and metagabbros or rodingites are mainly reworked during the S2 development (see Zanoni, Rebay & Spalla, 2016). In serpentinite, S2 is marked by Alpine HP–UHP mineral assemblages and is pre-dated by clinopyroxene porphyroclasts and amphibole-clinopyroxene-bearing vein nets (Fig. 2a), ascribable to the oceanic evolution, and by an S1 foliation (Fig. 2b) that represents the oldest detectable Alpine fabric (Rebay, Spalla & Zanoni, 2012; Zanoni, Rebay & Spalla, 2016). S1 foliation and up to millimetre-sized oceanic relics are also preserved in rodingites (Zanoni, Rebay & Spalla, 2016). S2 is

post-dated by localized ductile shear zones and by two groups of folds, represented by tight folds with west-dipping axial plane and a N–S shallow plunging axis (D3, Fig. 2d) and by open to gentle upright folds with shallow axis (D4), respectively. Among these latter two folding stages, the first is associated with the development of a differentiated axial plane foliation S3 that in serpentinites is marked by a mineral assemblage indicating low-pressure metamorphic conditions, representing the retrograde metamorphic re-equilibration during uplift (Rebay, Spalla & Zanoni, 2012).

4. Microstructures and mineral chemistry

Serpentinites have been divided into two groups on the basis of D2 parageneses – Ti-clinohumite-bearing and eclogite facies serpentinite – described in detail by Rebay, Spalla & Zanoni (2012). Pre-D2 minerals are represented by porphyroclasts of olivine1, clinopyroxene1 and Ti-clinohumite1 that are wrapped by S2 foliation (Fig. 3a). New mineral growths occur at the rims of clinopyroxene, Ti-clinohumite and olivine as fringes elongated parallel to S2 (Fig. 3a, b). The parageneses associated with D2 consist of olivine2, clinopyroxene2, antigorite ± Ti-clinohumite2 ± chlorite ± zircon (Fig. 3a, b), whereas post-D2 foliation is defined by serpentine, chlorite ± amphibole (Fig. 3c). A sample of eclogite facies serpentinite, collected north of Rayes de Proz (star in Fig. 1c), is characterized by pervasive S2 foliation, wrapping around clinopyroxene porphyroclasts (Fig. 3d–f) and relationships between mineral growth and S2 development are similar to those described above. Two generations of zircon (namely zircon1 and zircon2) are easily recognizable where pre-D2 cores consist of porphyroclasts rimmed by syn-D2 fringe-like overgrowths, aligned along S2 foliation (Fig. 3g). This texture is consistent with that of clinopyroxene, Ti-clinohumite and olivine from all serpentinite types (Fig. 3h). Larger zircon grains are at times boudinaged (Fig. 3i).

Compositions of olivine and clinopyroxene associated with pre-D2 and syn-D2 assemblages are different and distinctive, as detailed in Rebay, Spalla & Zanoni (2012). In summary, olivine cores and rims are very similar in composition, with a slight decrease in Mg towards the rims.

Clinopyroxene cores are Al- (up to 0.3 apfu), Ti- and Cr-rich and Ca-poor (0.8–0.92 apfu), whereas syn-D2 rims are Ca-rich (0.94–1 apfu) and Ti-, Cr- and Al-poor.

Syn-D2 serpentine has higher Mg (up to 11.45 apfu) and lower Fe (up to 0.9 apfu) and Al (up to 0.8 apfu) contents than pre-D2 serpentine. Based on the major-element compositional variations, using classical geothermobarometry and thermodynamic modelling, 2.5 ± 0.3 GPa and $600 \pm 20\,°C$ were estimated for the formation of mineral parageneses associated with D2 deformation stage (Rebay, Spalla & Zanoni, 2012).
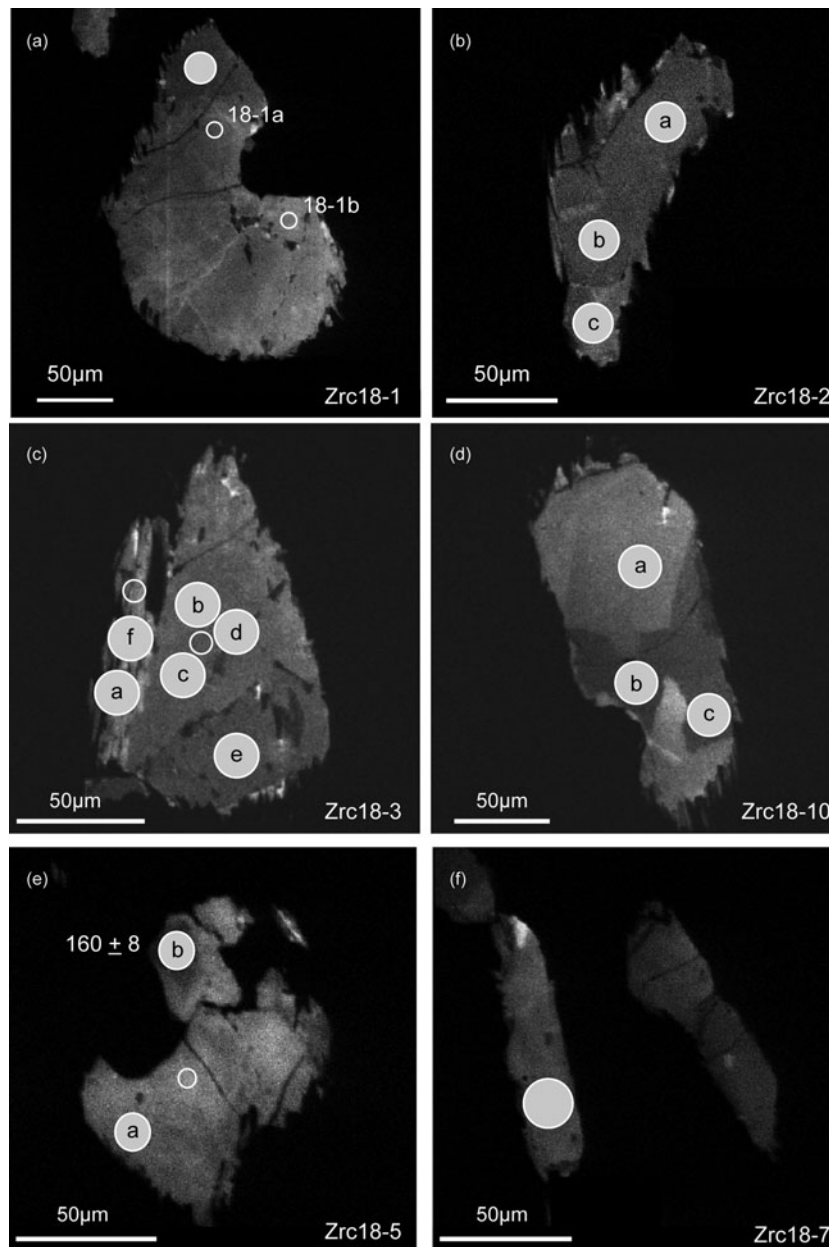
Figure 5. SEM images of zircon grains. (a–c) CL image of homogeneous zircon core with fringe-like syn-D2 overgrowth; (d) CL images of zircon grains showing sector and/or broad-banding zoning within cores and narrow rims with fringe-like syn-D2 overgrowth; (e, f) CL image of homogeneous zircon core with very few and tiny syn-S2 overgrowths; and (g–j, k–m) CL images of zircon grains showing sector and/or broad-banding zoning within cores and narrow rims with fringe-like syn-D2 overgrowth. Each image has the name of the zircon indicated and the large shaded circles indicate the spot analysed for U–Th–Pb geochronology, whereas smaller empty circles indicate spots analysed for trace elements. Letters differentiate circles in the same zircon, and correspond to the analyses in Tables 2 and 3. The concordant age of 168 ± 8 Ma obtained for zircon 18-5 spot b is also indicated in (e).

Clinopyroxene and zircon cores were analysed for trace-element composition with laser ablation (LA) ICP-MS (Table 2) at the CNR–IGG UOS of Pavia. The instrument couples a Nd:YAG laser working at 266 nm with a quadrupole ICP-MS (Perkin Elmer - DRCe). All analyses were carried out using a 10 μm spot (see online supplementary material, available at http://journals.cambridge.org/geo, for details on the analytical method).

The chondrite-normalized rare Earth element (REE) pattern (Fig. 4) of clinopyroxene is characterized by flat heavy REE (at about 100 times CI chondrite), a weak light REE depletion and negative Eu anomaly. Zr and Y concentrations are relatively high and are in the ranges 93.3–118 ppm and 402–449 ppm. The trace-element composition of zircon cores is characterized by low U concentration (9–18 ppm) and a chondrite-normalized REE pattern typical of growth under magmatic conditions, characterized by light REE depletion, positive Ce anomaly and heavy REE (HREE) enrichment (up to 3000 times CI chondrite). Zircon REE patterns parallel that of clinopyroxene for the occurrence of a negative Eu anomaly. Zircon fringe dimensions allowed only a single analysis.
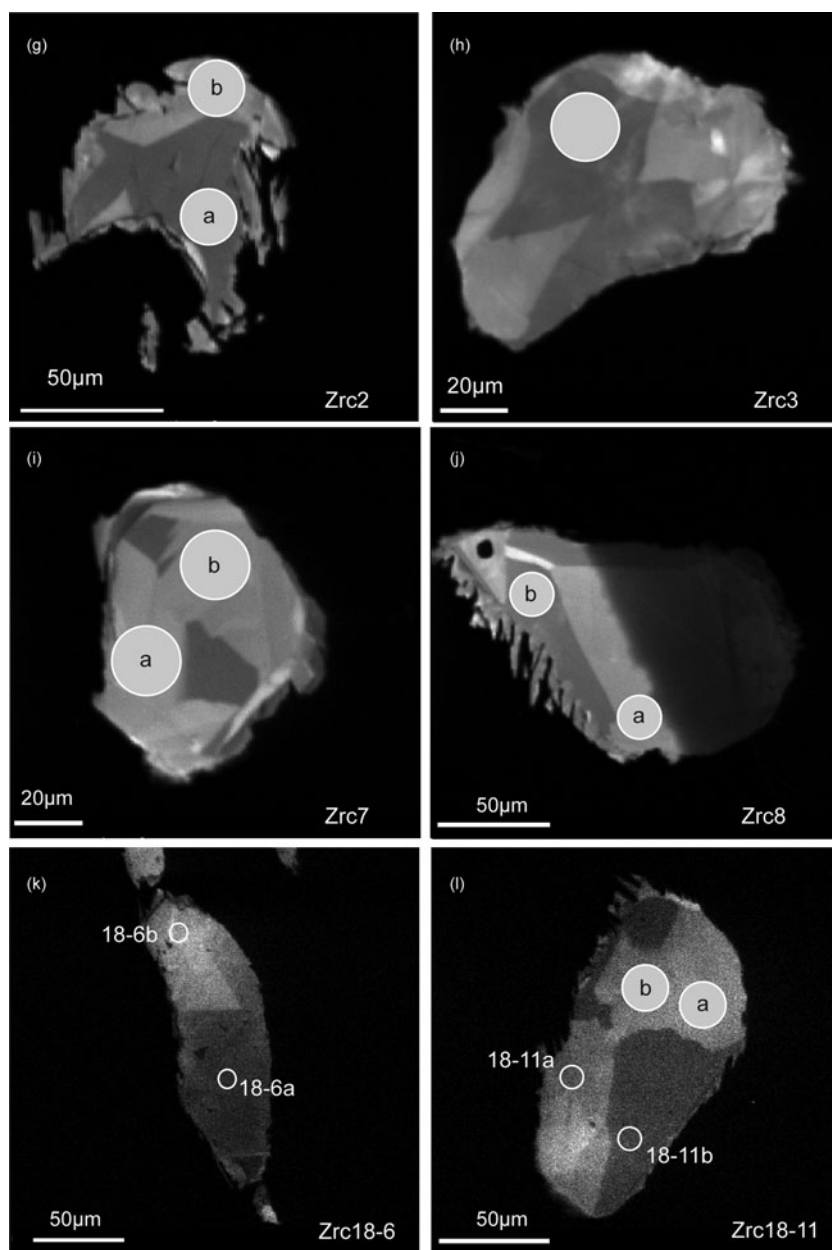
Figure 5. Continued

Trace-element composition of zircon fringes matches that of magmatic cores, revealing no significant difference in both REE contents and Th/U ratios. The absence of garnet and other mineral phases with high compatibility for REE (and other trace elements) in the HP–UHP mineral paragenesis in these rocks prevents their redistribution during zircon recrystallization, and accounts for the similar concentrations between magmatic cores and metamorphic rims.

5. U–Pb zircon geochronology

5.a. Method

U–Pb zircon geochronology was carried out with LA-ICP-MS on polished thin-sections at the CNR–IGG UOS of Pavia. The system couples an ArF excimer laser microprobe (type GeoLas102 from MicroLas) with a sector field ICP-MS (type Element from ThermoFinnigan). The signal of ^{202}Hg, ^{204}(Pb + Hg), ^{206}Pb, ^{207}Pb, ^{208}Pb, ^{232}Th and ^{238}U masses were acquired. ^{202}Hg is acquired to correct the isobaric interference of ^{204}Hg on ^{204}Pb, so that the common Pb in the sample can be monitored. The relatively high background at mass 204, due to trace of Hg in the He gas, prevents small amounts of common Pb being detected, however. Remarkably, in the investigated samples the signal of ^{204}(Pb + Hg) was always indistinguishable from the background and therefore no common Pb correction was applied. The ^{235}U signal is calculated from ^{238}U on the basis of the ratio ^{238}U/^{235}U = 137.818 (Hiess *et al.* 2012).

Laser-induced U–Pb fractionation and mass discrimination effects were simultaneously corrected

Table 3. Zircon isotopic data and apparent ages (zircon numbers refer to Fig. 5)

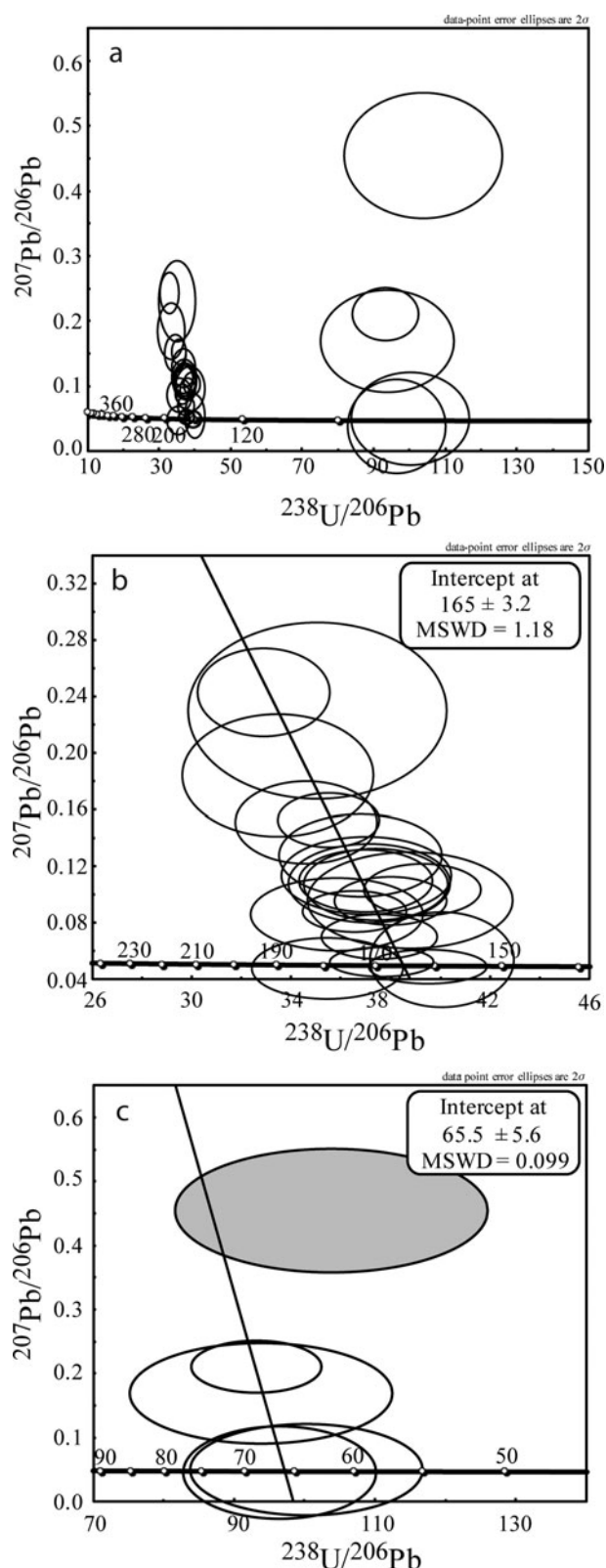| Identifier	Zrc#		Position	Cl	Isotope ratios						Apparent ages			
					$^{207}Pb/^{206}Pb$	2σ	$^{207}Pb/^{235}U$	2σ	$^{206}Pb/^{238}U$	2σ	$^{207}Pb/^{235}U$	2σ	$^{206}Pb/^{238}U$	2σ
Ju24a005	18-5	a	Core	Bright	0.0701	0.0135	0.2570	0.0485	0.0266	0.0013	232	44	169	9
Ju24a006	18-1		Core	Dark	0.1071	0.0226	0.3947	0.0803	0.0267	0.0017	338	69	170	11
Ju24a007	18-2	a	Rim	Dark	0.1526	0.0180	0.5925	0.0669	0.0282	0.0013	472	53	179	8
Ju24a008	18-2	b	Core	Dark	0.0962	0.0300	0.3422	0.1032	0.0258	0.0022	299	90	164	14
Ju24a009	18-2	c	Core	Bright/dark	0.1841	0.0423	0.7581	0.1621	0.0299	0.0028	573	122	190	18
Ju24a010	18-3	a	Rim	Bright	0.4551	0.1359	0.6044	0.1484	0.0096	0.0017	480	118	62	11
Ju24a011	18-3	b	Rim	Bright	0.1695	0.0744	0.2486	0.1020	0.0107	0.0017	225	93	68	11
Ju24a012	18-3	c	Core	Bright/dark	0.1036	0.0161	0.3635	0.0549	0.0255	0.0012	315	48	162	8
Ju24a013	18-3	d	Core	Dark	0.0954	0.0152	0.3461	0.0539	0.0263	0.0013	302	47	167	8
Ju24a014	18-3	e	Rim	Dark	0.1080	0.0248	0.4011	0.0889	0.0269	0.0019	342	76	171	12
Ju24a015	18-10	a	Core	Bright	0.0860	0.0231	0.3300	0.0859	0.0279	0.0022	290	75	177	14
Ju24a016	18-10	b	Core	Dark	0.0523	0.0090	0.1914	0.0326	0.0266	0.0012	178	30	169	8
Ju24a017	18-10	c	Core	Dark	0.1132	0.0251	0.4214	0.0893	0.0270	0.0020	357	76	172	13
Ju24a022	18-11	a	Core	Bright	0.1276	0.0268	0.4782	0.0957	0.0272	0.0020	397	79	173	13
Ju24a023	18-11	b	Core	Bright	0.1099	0.0197	0.4097	0.0709	0.0270	0.0016	349	60	172	10
Ju24a024	8	a	Core	Brigth	0.0881	0.0132	0.3323	0.0486	0.0274	0.0013	291	43	174	8
Ju24a025	8	b	Core	Dark	0.2311	0.0641	0.9054	0.2293	0.0285	0.0035	655	166	181	22
Ju24a026	3		Core	Dark	0.2431	0.0328	1.0193	0.1259	0.0304	0.0020	714	88	193	13
Ju24a027	2	a	Core	Dark	0.2108	0.0398	0.3116	0.0544	0.0107	0.0009	275	48	69	6
Ju24a028	7	a	Core	Bright	0.1510	0.0271	0.6015	0.1025	0.0289	0.0019	478	81	184	12
Ju24a029	7	b	Core	Bright	0.0477	0.0180	0.1853	0.0690	0.0282	0.0020	173	64	179	13
Ju24a034	2	b	Rim	Bright	0.0494	0.0591	0.0679	0.0808	0.0100	0.0013	64	79	67	9
Ju24a035	18-3	f	Rim	Bright	0.0460	0.0597	0.0657	0.0851	0.0104	0.0012	67	84	65	8
Ju24a036	18-5	b	Rim	Dark	0.0489	0.0105	0.1707	0.0361	0.0253	0.0013	161	34	160	8
Ju24a037	18-7		Rim	Dark	0.0540	0.0279	0.1860	0.0956	0.0250	0.0015	159	89	173	9

Figure 6. Tera-Wasserburg diagrams of isotopic ratios obtained from (a) all analysed zircon, (b) zircon cores and (c) syn-D2 overgrowths.

using a matrix-matched external standard and considering the same integration intervals on the standard and the unknowns. Analyses were carried out using a spot size of 20 μm and a laser fluence of 8 J cm^{-2}. The reference zircon GJ–1 (Jackson *et al.* 2004) was adopted as external standard and the reference zircons

91500 (Wiedenbeck *et al.* 1995) and 02123 (Ketchum *et al.* 2001) were selected as validation standards. Data reduction was carried out with the software package GLITTER® (van Achterbergh *et al.* 2001). Individual uncertainties given by the software for the isotope ratios were propagated relative to the respective reproducibility of the standard. This procedure was carried out for each analytical run as reported in Horstwood *et al.* (2003). ISOPLOT/Ex 3.00 software package by Ludwig (2003) was used for U–Pb apparent age calculations and representations. Data for external standards and validation standards are reported in online Supplementary Table S1 (available at http://journals.cambridge.org/geo).

5.b. Results

Zircon grains are generally prismatic and with dimensions up to 100 μm in length. They occur as porphyroclasts re-oriented parallel to S2 foliation. Zircon cores show mainly sector and broad banding zoning (Fig. 5d, g–l); homogeneous inner domains are also common (e.g. Fig. 5a–c, e–f). A peculiar feature, recognizable at the optical microscope (Fig. 3g) and well visible with CL imaging, is fringe-like tiny overgrowths elongated in the S2 HP–UHP foliation (Fig. 5a–d, g, j–l). Fringes are completely new portions of zircon without intergrowths with magmatic domains. Since the fringes are a few dozen microns in size, only those large enough to contain the spot were analysed. This selection avoided mixing rims with the inner (and older) cores, as confirmed by the consistency of the results and detailed in Figure 5, where the position of analyses is reported. Large zircons are frequently boudinaged (Fig. 3i); if zircon grains are separated into two or more fragments a narrow rim surrounds the different portions and is locally characterized by fringes parallel to S2 foliation, suggesting that boudinaging was coeval with the formation of these overgrowths (e.g. Fig. 5).

Eleven zircon grains were selected for analysis and 23 U–Pb data were collected. Isotopic ratios (Table 3) define two main arrays on the Tera-Wasserburg diagram (Fig. 6a). According to Compston (1999) the lower intercept of the array should fix the crystallization age, whereas the upper intercept defines the common Pb composition. The major cluster is from zircon cores and yields a lower intercept age at 165 ± 3.2 Ma (Fig. 6b). The minor cluster (four analyses) is from the tiny overgrowths and yields a lower intercept age at 65.5 ± 5.6 Ma (Fig. 6c).

6. Pressure–temperature–deformation–time (*P–T–d–t*) evolution and discussion

Textural features, mineral compositions and U–Pb geochronology allow additional constrains to be imposed on the two evolution steps witnessed by the ZSZ serpentinites and detailed in Rebay, Spalla & Zanoni (2012).
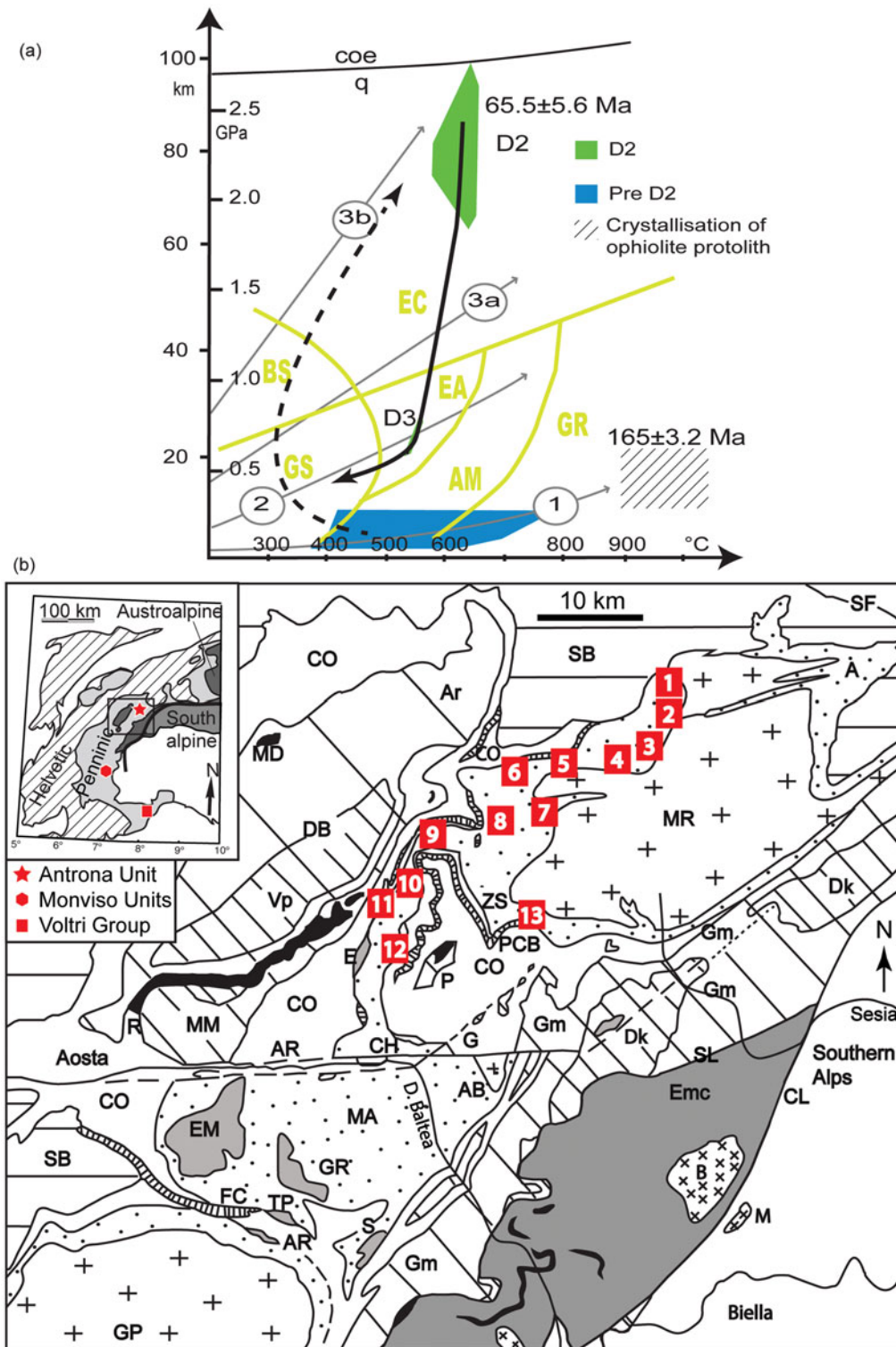
Figure 7. (Colour online) (a) *P–T–d–t* evolution of the studied ZSZ rocks synthesized from Rebay, Spalla & Zanoni (2012) and Zanoni, Rebay & Spalla (2016). Metamorphic facies are after Spear (1993). GS – greenschist; BS – blueschist; EC – eclogite; EA – epidote-amphibolite; AM – amphibolite; GR – granulite. Geotherms after Cloos (1993): (1) near spreading ridge or volcanic arc; (2) normal gradient of old plate interior; (3a) warm subduction zones; and (3b) cold subduction zones. (b) Tectonic sketch map of the northwestern Alps with the location of dated samples in the ZSZ. The inset shows the Western Alps with location of dated samples at Monviso. Nappe systems: Penninic continental nappe (MR – Monte Rosa; AB – Arcesa-Brusson; GP – Gran Paradiso; SB – Gran St Bernard); Austroalpine nappe (DB – Dent Blanche; MM – Mont Mary; P – Pillonet; AR – Acque Rosse; CH – Chatillon-St Vincent; E – Etirol-Levaz; G – Grun; EM – Mt Emilius; GR – Glacier-Refray; S – Santanel; TP – Tour Ponton; SL – Sesia-Lanzo Zone; Vp – Valpelline series; Dk – Diorite-kinzigitic series, Ar – Arolla series; Gm1 – Gneiss Minuti Complex, non-eclogitic; Gm2 – Gneiss Minuti Complex, with eclogitic relics; Emc – Eclogitic Micashist Complex; Mesozoic metasedimentary cover (black): R – Roisan Zone); and Ophiolite Piedmont Zone (CO – Combin Zone; PCB – Pancherot-Cime Bianche; FC – Faisceau de Cogne; ZS – Zermatt-Saas; MA – Mt Avic; A – Antrona ophiolite). Tectonic lines: CL – Canavese tectonic line; AR – Aosta-Ranzola fault system; SF – Simplon normal fault; MD – Mont Dolent; B – Biella; M – Miagliano; SC – Redrawn after Dal Piaz (1999).

Cores of the clinopyroxene and zircon porphyroclasts yield information on the protolith and more in general on the magmatic stage. The primary mineralogy of the rock is not preserved, so the identification of the rock type is not straightforward. Nonetheless, the negative Eu anomaly in both clinopyroxene and zircon (Fig. 4) suggests that the equilibrium melt already crystallized plagioclase. The abundant zircon and the relatively high concentrations of incompatible elements, such as Zr and Y, also suggest that the equilibrium melt was relatively evolved and not basaltic. Support for this conclusion is provided by the similar trace-element composition of analysed clinopyroxene as those from evolved lithologies of the Alpine Thetys such as the Fe–Ti oxide diorites (Tiepolo, Tribuzio & Vannucci, 1997). Textural and chemical features of zircon and clinopyroxene coupled to the overall mineralogy of the rock (olivine/serpentine-dominated) suggest that the evolved melt likely percolated/intruded the lithospheric mantle. The occurrence of gabbro bodies and rodingite dykes nearby support this conclusion. Processes of melt percolation and melt-rock reaction between the oceanic lithospheric mantle and melts with MORB affinity are well documented in both the Lanzo Massif (Piccardo, Zanetti & Müntener, 2007; Piccardo *et al.* 2007) and the Ligurian ophiolites (Sanfilippo, Tribuzio & Tiepolo, 2014). U–Pb geochronology yields a date of 165 ± 3.2 Ma for the zircon cores. Regarding mantle rocks, this date can either constrain the age of injection of the MORB-type melt into the mantle or the age of cooling of the oceanic lithosphere as a consequence of exhumation. Notwithstanding, the Middle Jurassic age is in perfect agreement with current knowledge on the age of formation of the Tethyan oceanic lithosphere in the Alps and Apennines (Rubatto, Gebauer & Fanning, 1998; Marotta *et al.* 2016; Tribuzio *et al.* 2016).

Both clinopyroxene and zircon porphyroclasts have rims and fringes parallel to the S2 foliation at the strain cap and shadow, respectively, which crystallized at *P–T* conditions of 2.2–2.8 GPa and 580–620 °C (Rebay, Spalla & Zanoni, 2012). The new U–Pb data reveal that this HP–UHP event, registered by the recrystallization of zircon rims and fringes at these *P–T* conditions, likely occurred at 65.5 ± 5.6 Ma and was followed by syn-D3 re-equilibration under epidote-amphibolite facies conditions (Fig. 7a; Rebay, Spalla & Zanoni, 2012; Zanoni, Rebay & Spalla, 2016). Radiometric ages obtained in this work extend the range 35–52 Ma reported in the literature for the Alpine HP–UHP re-equilibration towards older ages (Fig. 7b; Table 1). Remarkably, most of the literature ages have been obtained from samples that are within 20 km of the investigated area, and some are even nearer (≤5 km). Such geochronological heterogeneities imply that some sections of the ZSZ have likely experienced HP–UHP metamorphism earlier than previously thought; this supports the interpretation, based on contrasted *P–T* evolutions, that ZSZ is a complex containing different tectono-metamorphic units (e.g. Rebay, Spalla & Zanoni, 2012; Weber & Bucher, 2015). The new ages are comparable to those already reported for the HP re-equilibration in the subducted continental crust of the Sesia-Lanzo Zone, which records the oldest subduction ages among the tectonic units of the Western Alps (Rubatto, Gebauer & Compagnoni, 1999; Handy & Oberhänsli, 2004; Meda, Marotta & Spalla, 2010; Spalla *et al.* 2010; Cenki-Tok *et al.* 2011; Rubatto *et al.* 2011; Roda, Spalla & Marotta, 2012). Similar ages were also reported for the continental inliers of ZSZ (Beltrando, Rubatto & Manatschal, 2010; Weber *et al.* 2015; Fassmer *et al.* 2016).

Older ages interpreted as dating the *P–T* prograde evolution (Table 1; Skora *et al.* 2009, 2015) indicate that the subduction of ZSZ oceanic slices was already active at 80 Ma. Our data are therefore coherent with oceanic lithosphere subduction, necessary to justify the low thermal regime under which Western Alpine continental crust was exhumed (e.g. Zucali, Spalla & Gosso, 2002; Roda, Spalla & Marotta, 2012).

Scattered peak ages (41–72 Ma; Cliff, Barnicoat & Inger, 1998; Table 1) are also observed in the Monviso Massif, supporting the interpretation that it represents a complex of ophiolitic HP slices accreted during the final stages of their exhumation (Schwartz *et al.* 2000; Guillot *et al.* 2004). The detection of contrasted petrologic and chronologic histories in both the ZSZ and Monviso Massif confirms that the HP metaophiolites of Piedmont zone is a highly heterogeneous domain composed of slices of variable size, from one to tens of kilometres[3] (e.g. Guillot *et al.* 2004).

7. Conclusions

In summary, our results allow us to demonstrate that multiscale structural analysis assisted by detailed thermodynamic modelling is a fundamental tool for dating single deformation stages and associated mineral transformations.

The results confirm a Middle Jurassic age for oceanic crust accretion, which is in agreement with that observed in the ophiolitic complexes from the Alps and Apennines.

Finally, our results allow us to widen the time span under which rocks of ZSZ recorded HP–UHP conditions during 70–38 Ma and to infer that syn-D2 eclogite facies metamorphic imprint developed at 65.5 ± 5.6 Ma under a very low thermal regime, as suggested by the relationships with geotherm inferred by Cloos (1993) for cold subduction zones (Fig. 7). These findings go along with the cold thermal regime under which the Sesia-Lanzo Zone was exhumed, before intrusion of the Periadriatic magmas, which is compatible with ongoing oceanic subduction (e.g. Zucali, Spalla & Gosso, 2002; Zanoni, Spalla & Gosso, 2010; Roda, Spalla & Marotta, 2012; Roda & Zanoni, 2016).

Heterogeneous HP–UHP ages and contrasted *P–T–d–t* evolution within ZSZ can be explained either by: considering slices of ophiolites within a hydrated

mantle wedge that follow the same path at different times in a subduction system, where they can be tectonically sampled at different depths; or considering that they can follow different paths. These ophiolite slices can be coupled and/or decoupled at different times in a relatively long-lasting subduction system where oceanic and continental lithosphere are involved, as is the case for the Western Alps.

Declaration of interest

No conflict of interest exists for the authors.

Supplementary material

To view supplementary material for this article, please visit http://doi.org/10.1017/S0016756817000334

References

Amato, J. M., Johnson, C. M., Baumgartner, L. P. & Beard, B. L. 1999. Rapid exhumation of the Zermatt-Saas ophiolite deduced from high precision Sm-Nd and Rb-Sr geochronology. *Earth and Planetary Science Letters* **171**, 425–38.

Angiboust, S. & Agard, P. 2010. Initial water budget: the key to detaching large volumes of eclogitized oceanic crust along the subduction channel? *Lithos* **120**, 453–74.

Angiboust, S., Agard, P., Jolivet, L. & Beyssac, O. 2009. The Zermatt-Saas ophiolite: the largest (60-km wide) and deepest (c. 70–80 km) continuous slice of oceanic lithosphere detached from a subduction zone? *Terra Nova* **21**, 171–80.

Angiboust, S., Langdon, R., Agard, P., Waters, D. & Chopin, C. 2012. Eclogitization of the Monviso ophiolite (W. Alps) and implications on subduction dynamics. *Journal of Metamorphic Geology* **30**, 37–61.

Argand, E. 1911. Les nappes de recouvrement des Alpes Pennines et leurs prolongements structuraux. *Matériaux pour la Carte Géologique de la Suisse, n.s.* **31**, 1–26.

Barnicoat, A. C. 1988. Zoned high-pressure assemblages in pillow lavas of the Zermatt-Saas ophiolite zone, Switzerland. *Lithos* **21**, 227–36.

Barnicoat, A. C. & Fry, N. 1986. High pressure metamorphism of the Zermatt-Saas ophiolite zone, Switzer-

land. *Journal of the Geolological Society of London* **143**, 603–18.

Baumann, C., Gerya, T. V. & Connolly, J. A. D. 2010. Numerical modelling of spontaneous slab-breakoff dynamics during continental collision. In: *Advances in Interpretation of Geological Processes: Refinement of Multi-Scale Data and Integration in Numerical Modelling* (eds M. I. Spalla, A. M. Marotta & G. Gosso), pp. 99–114. Geological Society, London, Special Publication no. 332.

Bearth, P. 1967. Die ophiolite der Zone von Zermatt-Saas Fee. *Beitrag Geologische Karte Schweitz* **132**, 1–130.

Beltrando, M., Rubatto, D. & Manatschal, G. 2010. From passive margins to orogens: the link between ocean-continent transition zones and (ultra-)high-pressure metamorphism. *Geology* **38**(6), 559–62.

Bowtell, S. A., Cliff, R. A. & Barnicoat, A. C. 1994. Sm-Nd isotopic evidence on the age of eclogitization in the Zermatt-Saas ophiolite. *Journal of Metamorphic Geology* **12**, 187–96.

Brongniart, A. 1813. Essai d'une classification minéralogique des roches mélangées. *Journal des Mines* **XXXIV**, 190–9.

Bucher, K., Fazis, Y., de Capitani, C. & Grapes, R. 2005. Blueschists, eclogites, and decompression assemblages of the Zermatt-Saas ophiolite: high-pressure metamorphism of subducted Tethys lithosphere. *American Mineralogist* **90**, 821–35.

Bucher, K. & Frey, M. 1994. *Petrogenesis of Metamorphic Rocks*. Heidelberg, Berlin: Springer, 318 pp.

Bucher, K. & Grapes, R. 2009. The eclogite-facies Allalin gabbro of the Zermatt-Saas ophiolite, Western Alps: a record of subduction zone hydration. *Journal of Petrology* **50**, 1405–42.

Caron, J. M., Polino, R., Pognante, U., Lombardo, B., Lardeaux, J. M., Lagabrielle, Y., Gosso, G. & Allenbach, B. 1984. Ou sont les sutures majeures dans les Alpes internes? (transversale Briançon-Torino). *Memorie della Società Geologica Italiana* **29**, 71–8.

Cartwright, I. & Barnicoat, A. C. 2002. Petrology, geochronology, and tectonics of shear zones in the Zermatt-Saas and Combin zones of the Western Alps. *Journal of Metamorphic Geology* **20**, 263–81.

Cenki-Tok, B., Oliot, E., Rubatto, D., Berger, A., Engi, M., Janots, E., Thomsen, T. B., Manzotti, P., Regis, D., Spandler, C., Robyr, M. & Goncalves, P. 2011. Preservation of Permian allanite within an Alpine eclogite facies shear zone at Mt Mucrone, Italy: mechanical and chemical behavior of allanite during mylonitization. *Lithos* **125**, 40–50.

Chemenda, A. I., Mattauer, M., Malavieille, J. & Bokun, A. N. 1995. A mechanism for syn-collisional rock exhumation and associated normal faulting: results from physical modelling. *Earth and Planetary Science Letters* **132**, 225–32.

Chinner, G. A. & Dixon, J. E. 1973. Some high pressure parageneses of the Allalin gabbro, Valis, Switzerland. *Journal of Petrology* **14**, 185–202.

Cliff, R. A., Barnicoat, A. C. & Inger, S. 1998. Early Tertiary eclogite facies metamorphism in the Monviso ophiolite. *Journal of Metamophic Geology* **16**, 447–55.

Cloos, M. 1982. Flow melanges: numerical modelling and geological constraints on their origin in the Franciscan subduction complex. *Geological Society of America Bulletin* **93**, 330–45.

Cloos, M. 1993. Lithospheric buoyancy and collisional orogenesis: subduction of oceanic plateaus, continental

margins, island arcs, spreading ridges, and seamounts. *Geological Society of America Bulletin* **105**, 715–37.

COMPSTON, W. 1999. Geological age by instrumental analysis: the 29th Hallimond Lecture. *Mineralogical Magazine* **63**, 297–311.

DAL PIAZ, G. V. 1974. Le métamorphisme de haute pression et basse température dans l'évolution structurale du bassin ophiolitique alpino-apenninique. *Schweizerische Mineralogische und Petrographische Mitteilungen* **54**, 399–424.

DAL PIAZ, G. V. 1999. The Austroalpine-Piedmont nappe stack and the puzzle of Alpine Tethys. In *3rd Workshop on Alpine Geological Studies* (eds G. Gosso, F. Jadoul, M. Sella & M. I. Spalla), pp. 155–76. Societa Cooperativa Tipografica, Padua, Italy, Memorie di Scienze Geologiche.

DAL PIAZ, G. V. 2010. The Italian Alps: a journey across two centuries of Alpine geology. *Journal of the Virtual Explorer* **36**, paper 8, 1–108.

DAL PIAZ, G. V., CORTIANA, G., DEL MORO, A., MARTIN, S., PENNACCHIONI, G. & TARTAROTTI, P. 2001. Tertiary age and paleostructural inferences of the eclogitic imprint in the Austroalpine outliers and Zermatt-Saas Zone ophiolite, western Alps. *International Journal of Earth Sciences* **90**, 668–84.

DAL PIAZ, G. V. & ERNST, W. G. 1978. Areal geology and petrology of eclogites and associated metabasites of the Piemonte ophiolite nappe, Breuil – St. Jacques area, Italian Western Alps. *Tectonophysics* **51**, 99–126.

DAL PIAZ, G. V., VENTURELLI, G., SPADEA, P. & DI BATTISTINI, G. 1981. Geochemical features of metabasalts and metagabbros from the Piemonte ophiolite nappe, Italian Western Alps. *Neues Jahrbuch für Mineralogie - Abhandlungen* **142**, 248–69.

DALE, C. W., BURTON, K. W., PEARSON, D. G., GANNOUN, A., ALARD, O., ARGLES, T. W. & PARKINSON, I. J. 2009. Highly siderophile element behaviour accompanying subduction of oceanic crust: whole rock and mineral-scale insights from a high-pressure terrain. *Geochimica et Cosmochimica Acta* **73**, 1394–416.

DE GIUSTI, F., DAL PIAZ, G., V., SCHIAVO, A., MASSIRONI, M., MONOPOLI, B. & BISTACCHI, A. 2003. Carta geotettonica della Valle d'Aosta. *Memorie Di Scienze Geologiche* **55**, 129–49.

DE MEYER, C. M. C., BAUMGARTNER, L. P., BEARD, B. L. & JOHNSON, C. M. 2014. Rb–Sr ages from phengite inclusions in garnets from high pressure rocks of the Swiss Western Alps. *Earth and Planetary Science Letters* **395**, 205–16.

DUCHÊNE, S., BLICHERT-TOFT, J., LUAIS, B., TÉLOUK, P., LARDEAUX, J. M. & ALBARÈDE, F. 1997. The Lu-Hf dating of garnets and the ages of the Alpine high-pressure metamorphism. *Nature* **387**, 586–9.

ERNST, W. G. & DAL PIAZ, G. V. 1978. Mineral parageneses of eclogitic rocks and related mafic schists of the Piemonte ophiolite nappe, Breuil-St Jacques area, Italian Western Alps. *American Mineralogist* **63**, 621–40.

FASSMER, K., OBERMÜLLER, G., NAGEL, T. J., KIRST, F., FROITZHEIM, N., SANDMANN, S., MILADINOVA, I., FONSECA, R. O. C. & MÜNKER, C. 2016. High-pressure metamorphic age and significance of eclogite-facies continental fragments associated with oceanic lithosphere in the Western Alps (Etirol-Levaz Slice, Valtournenche, Italy). *Lithos* **252**, 145–59, doi:10.1016/j.lithos.2016.02.019.

FEDERICO, L., CAPPONI, G., CRISPINI, L., SCAMBELLURI, M. & VILLA, I. M. 2005. $^{39}Ar/^{40}Ar$ dating of high-pressure rocks from the Ligurian Alps: evidence for a continuous subduction–exhumation cycle. *Earth and Planetary Science Letters* **240**(3), 668–80.

FREZZOTTI, M. L., SELVERSTONE, J., SHARP, Z. D. & COMPAGNONI, R. 2011. Carbonate dissolution during subduction revealed by diamond-bearing rocks from the Alps. *Nature Geoscience* **4**, 703–6.

GERYA, T. V. 2011. Future directions in subduction modelling. *Journal of Geodynamics* **52**, 344–78.

GOUZU, C., ITAYA, T., HYODO, H. & MATSUDA, T. 2006. Excess 40Ar-free phengite in ultrahigh-pressure metamorphic rocks from the Lago di Cignana area, Western Alps. *Lithos* **92**(3–4), 418–30.

GOUZU, C., YAGI, K., THANH, N. X., ITAYA, T. & COMPAGNONI, R. 2016. White mica K–Ar geochronology of HP–UHP units in the Lago di Cignana area, western Alps, Italy: tectonic implications for exhumation. *Lithos* **248**, 109–18.

GROPPO, C., BELTRANDO, M. & COMPAGNONI, R. 2009. The P–T path of the ultra-high pressure Lago Di Cignana and adjoining high-pressure meta-ophiolitic units: insights into the evolution of the subducting Tethyan slab. *Journal of Metamorphic Geology* **27**, 207–31.

GUILLOT, S., SCHWARTZ, S., HATTORI, K., AUZENDE, A. & LARDEAUX, J. M. 2004. The Monviso ophiolitic massif (Western Alps), a section through a serpentinite subduction channel. *Journal of the Virtual Explorer* **16**, paper 3, 1–16.

HANDY, M. R. & OBERHÄNSLI, R. 2004. Explanatory notes to the map: metamorphic structures of the Alps age map of the metamorphic structure of the Alps – tectonic interpretation and outstanding problems. *Mitteilungen Österreichische Mineralogische Gesellschaft* **149**, 201–25.

HERWARTZ, D., MÜNKER, C., SCHERER, E. E., NAGEL, T. J., PLEUGER, J. & FROITZHEIM, N. 2008. Lu-Hf garnet geochronology of eclogites from the Balma Unit (Pennine Alps): implications for Alpine paleotectonic reconstructions. *Swiss Journal of Geosciences* **101**(S1), 173–89.

HIESS, J., CONDON, D. J., MCLEAN, N. & NOBLE, S. R. 2012. $^{238}U/^{235}U$ systematics in terrestrial Uranium-bearing minerals. *Geology* **335**, 1610–14.

HORSTWOOD, M. S. A., FOSTER, G. L., PARRISH, R. R., NOBLE, S. R. & NOWELL, G. M. 2003. Common-Pb corrected in situ U–Pb accessory mineral geochronology by LA–MC–CP–MS. *Journal of Analytical Atomic Spectrometry* **18**, 837–46.

JACKSON, S. E., PEARSON, N. J., GRIFFIN, W. L. & BELOUSOVA, E. 2004. The application of laser ablation inductively coupled plasma mass spectrometry to in situ U–Pb zircon geochronology. *Chemical Geology* **211**, 47–69.

KETCHUM, J. W. F., JACKSON, S. E., CULSHAW, N. G. & BARR, S. M. 2001. Depositional and tectonic setting of the Paleoproterozoic Lower Aillik Group, Makkovik Province, Canada: evolution of a passive margin-foredeep sequence based on petrochemistry and U-Pb (TIMS and LAM-ICP-MS) geochronology. *Precambrian Research* **105**, 331–56.

LAPEN, T. J., JOHNSON, C. M., BAUMGARTNER, L. P., MAHLEN, N. J., BEARD, B. L. & AMATO, J. M. 2003. Burial rates during prograde metamorphism of ultrahigh-pressure terrane: an example from Lago di Cignana, Western Alps, Italy. *Earth and Planetary Science Letters* **215**, 57–72.

LI, X. P., RAHN, M. K. & BUCHER, K. 2004. Serpentinites of the Zermatt-Saas ophiolite complex and their

texture evolution. *Journal of Metamorphic Geology* **22**, 159–77.

LIATI, A., FROITZHEIM, N. & FANNING, C. M. 2005. Jurassic ophiolites within the Valais domain of the Western and Central Alps: geochronological evidence for re-rifting of oceanic crust. *Contributions to Mineralogy and Petrology* **149**(4), 446–61.

LOMBARDO, B., RUBATTO, D. & CASTELLI, D. 2002. Ion microprobe U-Pb dating of zircon from a Monviso metaplagiogranite: implications for the evolution of the Piedmont-Liguria Tethys in the Western Alps. *Ofioliti* **27**(2), 109–17.

LUDWIG, K. R. 2003. Isoplot/Ex version 3.0: a geochronological toolkit for Microsoft Excel. Berkeley Geochronology Center Special Publication 4. Berkeley, Berkeley Geochronology Center, 70 pp.

MAHLEN, N. J., JOHNSON, C. M., BAUMGARTNER, L. P., LAPEN, T. J., SKORA, S. & BEARD, B. L. 2006. The protracted subduction history and HP/UHP metamorphism of the Zermatt–Saas ophiolite, western Alps, as constrained by Lu–Hf geochronology. In *EOS Transactions AGU Fall Meeting*, pp. V41E–05, San Francisco, 11–15 December 2006.

MALATESTA, C., CRISPINI, L., FEDERICO, L., CAPPONI, G. & SCAMBELLURI, M. 2012. The exhumation of high pressure ophiolites (Voltri Massif, Western Alps): insights from structural and petrologic data on metagabbro bodies. *Tectonophysics* **568–9**, 102–23.

MALATESTA, C., GERYA, T. V., CRISPINI, L., FEDERICO, L. & CAPPONI, G. 2016. Interplate deformation at early-stage oblique subduction: 3-D thermomechanical numerical modelling. *Tectonics* **35**(7), 1610–25, doi: 10.1002/2016TC004139.

MAROTTA, A. M., RODA, M., CONTE, K. & SPALLA, M. I. 2016. Thermo-mechanical numerical model of the transition from continental rifting to oceanic spreading: the case study of the Alpine Tethys. *Geological Magazine*, published online 3 October 2016, doi: 10.1017/S0016756816000856.

MARTIN, S., REBAY, G., KIENAST, J. R. & MEVEL, C. 2008. An ophiolitic palaeo-hydrothermal field metamorphosed in the eclogite-facies from the Italian western Alps, Saint Marcel valley. *Ofioliti* **33**, 49–63.

MEDA, M., MAROTTA, A. M. & SPALLA, M. I. 2010. The role of mantle hydration in continental crust recycling in the wedge region. In: *Advances in Interpretation of Geological Processes: Refinement of Multi-Scale Data and Integration in Numerical Modelling* (eds M. I. Spalla, A. M. Marotta & G. Gosso), pp. 149–72. Geological Society, London, Special Publication no. 332.

MEYER, J. 1983. Mineralogie und Petrologie des Allalingabbros. PhD thesis, Universitat Basel. Published thesis.

MONIÉ, P. & PHILIPPOT, P. 1989. Mise en évidence de l'âge éocène moyen du métamorphisme de haute-pression dans la nappe ophiolitique du Monviso (Alpes occidentales) par la méthode ^{39}Ar-^{40}Ar. *Comptes rendus de l'Académie des sciences. Série 2, Mécanique, Physique, Chimie, Sciences de l'univers, Sciences de la Terre* **309**(2), 245–51.

OBERHÄNSLI, R. 1980. PT bestimmungen anhand von mineralanalysen in eklogiten und glaukophaniten der ophiolite von Zermatt. *Schweizerische Mineralogische und Petrographische Mitteilungen* **60**, 215–35.

PICCARDO, G. B., ZANETTI, A. & MÜNTENER, O. 2007. Melt/peridotite interaction in the Southern Lanzo peridotite: Field, textural and geochemical evidence. *Lithos* **94**(1), 181–209.

PICCARDO, G. B., ZANETTI, A., PRUZZO, A. & PADOVANO, M. 2007. The North Lanzo peridotite body (NW Italy): lithospheric mantle percolated by MORB and alkaline melts. *Periodico di Mineralogia* **76**(2–3), 199–221.

POLINO, R., DAL PIAZ, G. V. & GOSSO, G. 1990. Tectonic erosion at the Adria margin and accretionary processes for the Cretaceous orogeny of the Alps. *Mémoires de la Société Géologique de France* **156**, 345–67.

REBAY, G., SPALLA, M. I. & ZANONI, D. 2012. Interaction of deformation and metamorphism during subduction and exhumation of hydrated oceanic mantle: insights from the Western Alps. *Journal of Metamorphic Geology* **30**, 687–702.

REDDY, S. M., WHEELER, J. & CLIFF, R. A. 1999. The geometry and timing of orogenic extension; an example from the Western Italian Alps. *Journal of Metamorphic Geology* **17**, 573–89.

REINECKE, T. 1991. Very high pressure metamorphism and uplift of coesite-bearing metasediments from the Zermatt-Saas Zone, Western Alps. *European Journal of Mineralogy* **10**, 7–17.

REINECKE, T. 1995. Ultrahigh and high-pressure metamorphic rocks of the Zermatt-Saas zone, Western Alps-records of burial and exhumation paths. *Bochumer Geologische und Geotechnische Arbeiten* **44**, 152–7.

REINECKE, T. 1998. Prograde high- to ultrahigh-pressure metamorphism and exhumation of oceanic sediments at Lago di Cignana, Zermatt-Saas zone, western Alps. *Lithos* **42**, 147–89.

RING, U. 1995. Horizontal contraction or horizontal extension? Heterogeneous late Eocene and early Oligocene general shearing during blueschist and greenschist facies metamorphism at the Pennine-Austroalpine boundary zone in the Western Alps. *Geologische Rundschau* **84**, 843–59.

RODA, M., MAROTTA, A. M. & SPALLA, M. I. 2010. Numerical simulations of an ocean-continent convergent system: influence of subduction geometry and mantle wedge hydration on crustal recycling. *Geochemistry, Geophysics, Geosystems* **11**, 1–21.

RODA, M., SPALLA, M. I. & MAROTTA, A. M. 2012. Integration of natural data within a numerical model of ablative subduction: a possible interpretation for the Alpine dynamics of the Austroalpine crust. *Journal of Metamorphic Geology* **30**, 973–96.

RODA, M. & ZANONI, D. 2016. Testing the thermal state of Biella pluton country rocks via numerical model of magma cooling. In *GeoMod 2016 Conference*, Montpellier, France, 17–20 October, p. 84–5.

RUBATTO, D., GEBAUER, D. & COMPAGNONI, R. 1999. Dating of eclogite facies zircons: the age of Alpine metamorphism in the Sesia–Lanzo Zone (Western Alps). *Earth and Planetary Sciences Letters* **167**, 141–58.

RUBATTO, D., GEBAUER, D. & FANNING, M. 1998. Jurassic formation and Eocene subduction of the Zermatt-Saas-Fee ophiolites: implications for the geodynamic evolution of the Central and Western Alps. *Contributions to Mineralogy and Petrology* **132**, 269–87.

RUBATTO, D., REGIS, D., HERMANN, J., BOSTON, K., ENGI, M., BELTRANDO, M. & MCALPINE, S. R. B. 2011. Yo-yo subduction recorded by accessory minerals in the Italian Western Alps. *Nature Geoscience* **4**(5), 338–42.

RUBATTO, R. & HERMANN, J. 2003. Zircon formation during fluid circulation in eclogites (Monviso, Western Alps): Implications for Zr and Hf budget in subduction zones. *Geochimica et Cosmochimica Acta* **67**, 2173–87.

SANFILIPPO, A., TRIBUZIO, R. & TIEPOLO, M. 2014. Mantle-crust interaction in the oceanic lithosphere: constraints

from minor and trace elements in olivine. *Geochimica et Cosmochimica Acta* **141**, 423–39.

SCHWARTZ, S., LARDEAUX, J. M., GUILLOT, S. & TRICART, P. 2000. Diversité du métamorphisme éclogitique dans le massif ophiolitique du Monviso (Alpes Occidentales, Italie). *Geodinamica Acta* **13**, 169–88.

SKORA, S., LAPEN, T. J., BAUMGARTNER, L. P., JOHNSON, C. M., HELLEBRAND, E. & MAHLEN, N. J. 2009. The duration of prograde garnet crystallization in the UHP eclogites at Lago di Cignana, Italy. *Earth and Planetary Science Letters* **287**, 402–11.

SKORA, S., MAHLEN, N. J., JOHNSON, C. M., BAUMGARTNER, L. P., LAPEN, T. J., BEARD, B. L. & SZILVAGYI, E. T. 2015. Evidence for protracted prograde metamorphism followed by rapid exhumation of the Zermatt-Saas Fee ophiolite. *Journal of Metamorphic Geology* **33**, 711–34.

SPALLA, M. I., GOSSO, G., MAROTTA, A. M., ZUCALI, M. & SALVI, F. 2010. Analysis of natural tectonic systems coupled with numerical modelling of the polycyclic continental lithosphere of the Alps. *International Geology Review* **52**, 1268–302.

SPEAR, F. S. 1993. *Metamorphic Phase Equilibria and Pressure-Temperature-Time Paths*. Mineralogical Society of America, Chelsea, Michigan: BookCrafters, Inc., 799 pp.

SPRINGER, K., LAPEN, T. J., BAUMGARTNER, L. P., JOHNSON, C. M. & BEARD, B. L. 2009. Sm-Nd geochronology of the Zermatt-Saas ophiolite, northern Italy. *Geochimica et Cosmochimica Acta* (Supplement) **73**, p. A1258.

STEINMANN, G. 1927. Die ophiolitshen zonen in den mediterranen Kettengebirgen, translated and reprinted by Bernoulli and Friedman. In *Ophiolite Concept and the Evolution of Geologic Thought* (eds Y. Dilek & S. Newcomb), pp. 77–91. Geological Society of America, Special Publication, 373.

STOECKHERT, B. & GERYA, T. 2005. Pre-collisional high pressure metamorphism and nappe tectonics at active continental margins: a numerical simulation. *Terra Nova* **17**, 102–10.

TIEPOLO, M., TRIBUZIO, R. & VANNUCCI, R. 1997. Mg- and Fe-gabbroids from Northern Apennine ophiolites: Parental liquids and igneous differentiation process. *Ofioliti* **22**, 57–70.

TRIBUZIO, R., GARZETTI, F., CORFU, F., TIEPOLO, M. & RENNA, M. R. 2016. U–Pb zircon geochronology of the Ligurian ophiolites (Northern Apennine, Italy): Implications for continental breakup to slow seafloor spreading. *Tectonophysics* **666**, 220–43.

VAN ACHTERBERGH, E., RYAN, C. G., JACKSON, S. E. & GRIFFIN, W. 2001. Data reduction software for LA-ICPMS. In *Laser ablation ICPMS in the Earth Sciences: Principles and Applications* (ed. P. Sylvester), pp. 239–43. Mineralogical Association of Canada, Short Course Series 29.

VAN DER KLAUW, S. N. G. C., REINECKE, T. & STÖCKHERT, B. 1997. Exhumation of ultrahigh-pressure metamorphic oceanic crust from Lago di Cignana, Piemontese zone, Western Alps. *Lithos* **41**, 79–102.

WEBER, S. & BUCHER, K. 2015. An eclogite-bearing continental tectonic slice in the Zermatt–Saas high-pressure ophiolites at Trockener Steg (Zermatt, Swiss Western Alps). *Lithos* **232** 336–59.

WEBER, S., SANDMANN, S., MILADINOVA, I., FONSECA, R. O. C., FROITZHEIM, N., MÜNKER, C. & BUCHER, K. 2015. Dating the initiation of Piemonte-Liguria Ocean subduction: Lu–Hf garnet chronometry of eclogites from the Theodul Glacier Unit (Zermatt-Saas zone, Switzerland). *Swiss Journal of Geosciences* **108**, 183–99, doi: 10.1007/s00015-015-0180-5.

WIEDENBECK, M., ALLÉ, P., CORFU, F., GRIFFIN, W. L., MEIER, M., OBERLI, F., VON QUADT, A., RODDICK, J. C. & SPIEGEL, W. 1995. Three natural zircon standards for U–Th–Pb, Lu–Hf, trace elements and REE analyses. *Geostandards Newsletter* **19**, 1–23.

ZANONI, D., REBAY, G., BERNARDONI, J. & SPALLA, M. I. 2012. Using multiscale structural analysis to infer high-/ultrahigh-pressure assemblages in subducted rodingites of the Zermatt-Saas Zone at Valtournanche, Italy. In *Multiscale Structures and Tectonic Trajectories in Active Margins* (eds M. Zucali, M. I. Spalla & G. Gosso), paper 6. *Journal of the Virtual Explorer* **41**.

ZANONI, D., REBAY, G. & SPALLA, M. I. 2016. Ocean floor and subduction record in the Zermatt-Saas rodingites, Valtournanche, Western Alps. *Journal of Metamorphic Geology* **34**, 941–961. doi: 10.1111/jmg.12215.

ZANONI, D., SPALLA, M. I. & GOSSO, G. 2010. Structure and PT estimates across late-collisional plutons: constraints on the exhumation of western Alpine continental HP units. *International Geology Review* **52**(10–12), 1244–67.

ZUCALI, M., SPALLA, M. I. & GOSSO, G. 2002. Strain partitioning and fabric evolution as a correlation tool: the example of the eclogitic micaschists complex in the Sesia-Lanzo Zone (Monte Mucrone–Monte Mars, Western Alps Italy). *Schweizerische Mineralogische und Petrographische Mitteilungen* **82**, 429–54.